

INF-SUP STABILIZED SCOTT–VOGELIUS PAIRS ON GENERAL SIMPLICIAL GRIDS FOR NAVIER–STOKES EQUATIONS

NAVEED AHMED, VOLKER JOHN, XU LI, AND CHRISTIAN MERDON

ABSTRACT. This paper considers the discretization of the time-dependent Navier–Stokes equations with the family of inf-sup stabilized Scott–Vogelius pairs recently introduced in [John/Li/Merdon/Rui, [arXiv:2206.01242](#), 2022] for the Stokes problem. Therein, the velocity space is obtained by enriching the \mathbf{H}^1 -conforming Lagrange element space with some $\mathbf{H}(\text{div})$ -conforming Raviart–Thomas functions, such that the divergence constraint is satisfied exactly. In these methods arbitrary shape-regular simplicial grids can be used.

In the present paper two alternatives for discretizing the convective terms are considered. One variant leads to a scheme that still only involves volume integrals, and the other variant employs upwinding known from DG schemes. Both variants ensure the conservation of linear momentum and angular momentum in some suitable sense. In addition, a pressure-robust and convection-robust velocity error estimate is derived, i.e., the velocity error bound does not depend on the pressure and the constant in the error bound for the kinetic energy does not blow up for small viscosity. After condensation of the enrichment unknowns and all non-constant pressure unknowns, the method can be reduced to a $\mathbf{P}_k - P_0$ -like system for arbitrary velocity polynomial degree k . Numerical studies verify the theoretical findings.

1. INTRODUCTION

Incompressible flows are modeled by the transient Navier–Stokes equations and seek a velocity \mathbf{u} and pressure p such that

$$(1.1) \quad \begin{aligned} \partial_t \mathbf{u} + (\mathbf{u} \cdot \nabla) \mathbf{u} - \nu \Delta \mathbf{u} + \nabla p &= \mathbf{f} && \text{in } (0, T] \times \Omega, \\ \text{div}(\mathbf{u}) &= 0 && \text{in } (0, T] \times \Omega, \\ \mathbf{u}(0) &= \mathbf{u}^0 && \text{in } \Omega, \\ \mathbf{u} &= \mathbf{0} && \text{on } (0, T] \times \partial\Omega, \end{aligned}$$

in a bounded Lipschitz domain $\Omega \subset \mathbb{R}^d$, $d \in \{2, 3\}$, and for a given $T < \infty$. The given data $\nu \in \mathbb{R}$, \mathbf{f} , and \mathbf{u}^0 denote the dimensionless viscosity, the external force, and the initial velocity, respectively. Note that problem (1.1) is already given in a dimensionless form. For simplicity, it is assumed that $\mathbf{f} \in L^2(0, T; \mathbf{L}^2(\Omega))$. The method under consideration is based on a classical weak formulation for (1.1): Find $(\mathbf{u}, p) : (0, T] \rightarrow \mathbf{V} \times Q := \mathbf{H}_0^1(\Omega) \times L_0^2(\Omega)$ such that

$$(1.2) \quad \begin{aligned} (\partial_t \mathbf{u}, \mathbf{v}) + ((\mathbf{u} \cdot \nabla) \mathbf{u}, \mathbf{v}) + (\nu \nabla \mathbf{u}, \nabla \mathbf{v}) - (\text{div}(\mathbf{v}), p) &= (\mathbf{f}, \mathbf{v}) && \forall \mathbf{v} \in \mathbf{V}, \\ (\text{div}(\mathbf{u}), q) &= 0 && \forall q \in Q, \end{aligned}$$

and $\mathbf{u}(0) = \mathbf{u}^0$. Here, $\mathbf{H}_0^1(\Omega) := [H_0^1(\Omega)]^d$ with $H_0^1(\Omega)$ being the Sobolev space of functions in $H^1(\Omega)$ with zero trace along $\partial\Omega$. The space $L_0^2(\Omega)$ collects all functions in $L^2(\Omega)$ with zero mean, and (\bullet, \bullet) denotes the usual L^2 inner product.

2020 *Mathematics Subject Classification.* 76D05, 76M10, 65M60.

Key words and phrases. Navier–Stokes equations, finite element methods, divergence-free, pressure-robust, convection-robust, a priori bounds.

Developing physically consistent schemes for (1.1) or (1.2), in the meanings described next, is a challenging topic, since there are several invariant structural (physical) properties or balance laws to be taken into account. They comprise the pointwise conservation of mass (i.e., the divergence-free property of the velocity), and the balance laws of kinetic energy, linear momentum, angular momentum, enstrophy, vorticity and helicity [37, 15, 9]. Moreover, there is an invariance property that the velocity field is independent from any gradient field force [33, 35, 26]. All these properties are considered to be crucial in designing physically consistent numerical schemes. Simultaneously, from the mathematical point of view, one has to consider discrete inf-sup stability and the continuity requirement when choosing discrete space pairs (\mathbf{V}_h, Q_h) . Combining the physical and mathematical requests is a challenging endeavor, since it is well known that some aspects of the physical consistency and the satisfaction of the discrete inf-sup condition have competing requirements. For some remarkable explorations in this regard, we refer to the divergence-free finite element methods [47, 13, 49, 48, 15, 19, 20, 21], pressure-robust reconstruction methods [33, 34, 36, 28, 3], EMAC formulation [9, 39, 10], and other structure-preserving methods such as [1, 42, 41, 4].

Among the physical properties mentioned above, the preservation of mass is strongly related to the other properties. On the one hand, it has been shown in [15, 9] that \mathbf{H}^1 -conforming divergence-free methods preserve proper balance of kinetic energy, linear momentum and angular momentum in some appropriate sense. Similar properties for $\mathbf{H}(\text{div})$ -conforming divergence-free discontinuous Galerkin (DG) methods can be also found in [11], except that there is some artificial dissipation if upwind fluxes are chosen, which modifies the balance of energy. However, it is also well-known that the upwind fluxes can have even much better performance than central fluxes with respect to the convergence order [22, 23]. Also the pressure-robustness property, which means that the velocity error is independent of the pressure, is usually ensured by a divergence-free method, if no consistency errors arise from the inner product with the force term [26]. Finally, the divergence-free property is also related to another important property called Re-semi-robustness or convection-robustness [45, 16], which means that the constants (including the Gronwall constant) in the error estimates of the kinetic energy do not depend on the inverse of the viscosity explicitly. It was shown in [45, 16] that a large class of divergence-free \mathbf{H}^1 -conforming and $\mathbf{H}(\text{div})$ -conforming methods is convection-robust with convergence order k , where k is the order of velocity space.

The starting point of this paper is the family of divergence-free elements designed in [32, 25] for the incompressible Stokes problem. This family is easy to implement, divergence-free and inf-sup stable on general shape-regular simplicial meshes. The main idea is to employ $\mathbf{H}(\text{div})$ -conforming Raviart–Thomas bubbles to enrich the generally non-inf-sup stable Scott–Vogelius finite element pair $\mathbf{P}_k - P_{k-1}^{\text{disc}}$. Here, \mathbf{P}_k denotes the vector-valued space of continuous piecewise polynomials of order k and P_{k-1}^{disc} denotes the scalar spaces of discontinuous piecewise polynomials of order $k - 1$.

Thus, the enriched velocity space consists of a classical \mathbf{H}^1 -conforming part and a (small) $\mathbf{H}(\text{div})$ -conforming part. It combines the advantages of divergence-free \mathbf{H}^1 -conforming and $\mathbf{H}(\text{div})$ -conforming methods: compared to the pure divergence-free \mathbf{H}^1 -conforming methods on general meshes [19, 20, 12], the relaxation of the continuity requirement of the bubble part allows a much simpler construction and implementation; opposite to pure $\mathbf{H}(\text{div})$ -conforming schemes [13, 46, 5], the new formulation only consists of volume integrals, and for $k \geq d$ the scheme is parameter-free for the Stokes problem. Moreover, similarly to the HDG schemes [29, 30, 27], the proposed methods can be reduced to a $\mathbf{P}_k - P_0$ problem via static condensation, for any $k \geq 1$, in this way decreasing the dimension of the global problem notably.

The goal of the present paper consists in extending the methods from [32, 25] from the steady-state Stokes equations to the transient Navier–Stokes equations, with particular consideration of the above mentioned physical properties. It will be shown that the suggested schemes have similar properties as pure divergence-free \mathbf{H}^1 -conforming or $\mathbf{H}(\text{div})$ -conforming methods in the sense that they preserve linear momentum and angular momentum, satisfy pressure-robustness and they are convection-robust. In addition, they maintain most of the particular advantages mentioned before for the Stokes case.

The main difficulty for achieving all these favorable properties is the discretization of the convection term, which requires a careful design. On the one hand, since \mathbf{H}^1 -conforming elements are also $\mathbf{H}(\text{div})$ -conforming, the upwind $\mathbf{H}(\text{div})$ -conforming DG formulation is one possible choice. On the other hand, if the convective term is treated implicitly, the face integrals of the DG upwinding increase the coupling of degrees of freedom, which compromises some of the original advantages and motivations in [32, 25]. Another possible choice is motivated by [31], where a structure-preserving convective formulation was proposed for the pressure-robust reconstruction schemes of [36]. A similar formulation is proposed here, which consists of volume integrals only. We like to emphasize that there is a fundamental difference between the method studied here and the one in [36, 31]. The former is indeed a nonconforming divergence-free method and the latter one is a conforming, but non-divergence-free method with reconstruction. In the present paper both choices for the convection term are analyzed. The analysis of the convection form inspired by [31] suggests to add one of two stabilizations for the $\mathbf{H}(\text{div})$ -conforming part to improve the error bounds. One of them is proposed in [31], and interestingly, for $k \geq d$, the other one is similar to a grad-div stabilization [38, 40, 8, 14] despite the different purpose.

Finally, it should be stressed that compared to the method in [31], the novel methods possess some features that are of particular interest in practice. They compute an exactly divergence-free velocity solution, which means that the mass is conserved pointwise. Moreover, the method in [31] uses classical pressure-discontinuous Stokes elements whose bubbles are polynomials of higher order, that require higher order quadrature rules especially in three dimensions. The methods suggested in the present paper keep the polynomial order k for all ansatz functions in any dimensions. Most importantly, these methods are able to be reduced to a $\mathbf{P}_k - P_0$ system due to the special construction of the enrichment and divergence constraint, so that the dimension of the global problem is reduced notably.

The remainder of the paper is organized as follows. Section 2 introduces the notation and describes the involved finite element spaces. Section 3 presents and discusses two discrete formulations of the Navier–Stokes problem and analyzes conservation or balance properties for kinetic energy, linear momentum, and angular momentum. A pressure-robust and convection-robust error estimate for the time-continuous discrete schemes is given in Section 4. Section 5 discusses the possibility to reduce the scheme to a $\mathbf{P}_k - P_0$ system. Section 6 reports on some numerical studies that verify the convection-robust convergence order and illustrate the overall performance of the proposed methods in some benchmark problems, such as the classical Kelvin–Helmholtz instability. Section 7 draws some conclusions and gives an outlook on aspects that deserve further attention in the future.

2. PRELIMINARIES

This section introduces the notation and recalls the main ideas of the proposed Raviart–Thomas enrichment spaces for the Scott–Vogelius finite element pairs from [32, 25].

2.1. Notation. Consider a regular triangulation into simplices \mathcal{T} of the domain Ω with nodes \mathcal{N} and facets \mathcal{F} . The subset \mathcal{F}^0 denotes all interior faces. The diameter of an element $T \in \mathcal{T}$ is denoted by h_T and gives rise to the local mesh-width function $h_{\mathcal{T}}$ via $h_{\mathcal{T}}|_T := h_T$ for all $T \in \mathcal{T}$. The maximum mesh-width is given by $h := \max_{T \in \mathcal{T}} h_T$. The vector \mathbf{n}_T defines the outer unit normal vector along the boundary ∂T of a simplex $T \in \mathcal{T}$. On a face F , the notation $[[\bullet]]$ denotes the jump of \bullet and $\{\{\bullet\}\}$ denotes its average value.

On a subdomain ω , the space of all scalar-valued polynomials of order k on ω is denoted by $P_k(\omega)$ and is written in bold, i.e., $\mathbf{P}_k(\omega)$, in case of vector-valued polynomials. Piecewise continuous and discontinuous polynomial spaces with respect to the triangulation are given by

$$\begin{aligned} P_k(\mathcal{T}) &:= \left\{ q_h \in H^1(\Omega) : q_h|_T \in P_k(T) \text{ for all } T \in \mathcal{T} \right\}, \\ P_k^{\text{disc}}(\mathcal{T}) &:= \left\{ q_h \in L^2(\Omega) : q_h|_T \in P_k(T) \text{ for all } T \in \mathcal{T} \right\}. \end{aligned}$$

The suggested enrichment relies on specially chosen Raviart–Thomas function. The space of all Raviart–Thomas functions of order k on a cell $T \in \mathcal{T}$ is given by

$$\mathbf{RT}_k(T) := \left\{ \mathbf{v} \in \mathbf{L}^2(T) : \exists \mathbf{p} \in \mathbf{P}_k(T), q \in P_k(T), \mathbf{v}|_T(\mathbf{x}) = \mathbf{p}(\mathbf{x}) + q(\mathbf{x})\mathbf{x} \right\}.$$

Their $H(\text{div})$ -conforming combinations define the global space

$$\mathbf{RT}_k(\mathcal{T}) := \{ \mathbf{v} \in \mathbf{H}(\text{div}, \Omega) : \forall T \in \mathcal{T} \mathbf{v}|_T \in \mathbf{RT}_k(T) \}.$$

The subspace of interior Raviart–Thomas bubble functions reads

$$\mathbf{RT}_k^{\text{int}}(\mathcal{T}) := \{ \mathbf{v} \in \mathbf{RT}_k(\mathcal{T}) : \mathbf{v} \cdot \mathbf{n}_T|_{\partial T} = 0 \text{ for all } T \in \mathcal{T} \}.$$

This space can be further decomposed into

$$\mathbf{RT}_k^{\text{int}}(\mathcal{T}) = \mathbf{RT}_{k,0}^{\text{int}}(\mathcal{T}) \oplus \widetilde{\mathbf{RT}}_k^{\text{int}}(\mathcal{T}),$$

where the first part consists of only divergence-free functions and the second part $\widetilde{\mathbf{RT}}_k^{\text{int}}(\mathcal{T})$ is its arbitrary but fixed complement space. Then, since the only divergence-free function in $\widetilde{\mathbf{RT}}_k^{\text{int}}(\mathcal{T})$ is the zero function, the divergence operator on this space is injective and allows the following estimate under a mild requirement in Remark 2.2.

Lemma 2.1 ([25]). *For any $\mathbf{v}_h \in \widetilde{\mathbf{RT}}_k^{\text{int}}(\mathcal{T})$, there holds the inequality*

$$(2.1) \quad \|\mathbf{v}_h\|_{\mathbf{L}^2(T)} \leq Ch_T \|\text{div}(\mathbf{v}_h)\|_{L^2(T)} \quad \text{for all } T \in \mathcal{T}.$$

Remark 2.2. *In general, the space $\widetilde{\mathbf{RT}}_k^{\text{int}}(\mathcal{T})$ is not unique for $k > 1$. We only require that it breaks into local spaces $\widetilde{\mathbf{RT}}_k^{\text{int}}(T), T \in \mathcal{T}$, that have the same structure in the sense that all of them are connected to the same reference space via Piola’s transformation (see e.g. [6, Eq. 2.1.69]). Since these spaces are characterized by the normal trace and the divergence, which are preserved (in a scaled meaning) by Piola’s transformation, this requirement is natural.*

Furthermore, the subspace of elementwise zero-mean functions in $P_k^{\text{disc}}(\mathcal{T})$ reads

$$(2.2) \quad \widetilde{P}_k^{\text{disc}}(\mathcal{T}) := \left\{ q_h \in P_k^{\text{disc}}(\mathcal{T}) : (q_h, 1)_T = 0 \text{ for all } T \in \mathcal{T} \right\}.$$

For $k = 0$, one obtains $\mathbf{RT}_0^{\text{int}}(\mathcal{T}) = \widetilde{\mathbf{RT}}_0^{\text{int}}(\mathcal{T}) = \{\mathbf{0}\}$ and $\widetilde{P}_0^{\text{disc}}(\mathcal{T}) = \{0\}$. It also holds $\mathbf{RT}_1^{\text{int}}(\mathcal{T}) = \widetilde{\mathbf{RT}}_1^{\text{int}}(\mathcal{T})$ because there is no divergence-free interior bubble in \mathbf{RT}_1 .

Throughout this paper, for any (scalar or vector-valued) finite element space \mathcal{S} (with or without an argument like \mathcal{T}), its local version on each element T is denoted by $\mathcal{S}(T)$ if not specially indicated. The symbol $\pi_{\mathcal{S}}$ (or $\pi_{\mathcal{S}(T)}$) denotes the L^2 projection operator onto \mathcal{S} (or $\mathcal{S}(T)$, respectively). $\|\bullet\|_{W^{m,p}(\omega)}$ is used to denote the $W^{m,p}$ Sobolev norm of \bullet on the domain ω . By convention, ω is omitted if $\omega = \Omega$, and the L^2 norm of \bullet is then simply denoted by $\|\bullet\|$.

2.2. Raviart–Thomas enriched Scott–Vogelius finite element pair. For $k \geq 1$, consider the \mathbf{H}^1 -conforming velocity ansatz space of piecewise vector-valued polynomials

$$\mathbf{V}_h^{\text{ct}} := \mathbf{P}_k(\mathcal{T}) \cap \mathbf{V}$$

and the desired pressure space

$$Q_h := P_{k-1}^{\text{disc}}(\mathcal{T}) \cap Q.$$

These are the ansatz spaces for the classical Scott–Vogelius finite element method which are known to be not inf-sup stable in general. The main idea of [32, 25] is to enrich the velocity spaces by some specially chosen Raviart–Thomas functions collected in the space \mathbf{V}_h^{R} . The characteristic property of \mathbf{V}_h^{R} is that

$$\text{div}(\mathbf{V}_h^{\text{R}}) \oplus_{L^2} \widehat{Q}_h = Q_h$$

such that $\mathbf{V}_h^{\text{ct}} \times \widehat{Q}_h$ is inf-sup stable for some subspace $\widehat{Q}_h \subseteq Q_h$. The choice of \widehat{Q}_h is not unique in general. Suggested by [25], well-known inf-sup stability results from literature [6, 24] allow to use $\widehat{Q}_h = P_{k-d}^{\text{disc}}(\mathcal{T}) \cap Q$ for $k \geq d$ and $\widehat{Q}_h = \{0\}$ for $k < d$. The corresponding Raviart–Thomas enrichment space \mathbf{V}_h^{R} reads

$$(2.3) \quad \mathbf{V}_h^{\text{R}} = \begin{cases} \mathbf{RT}_0(\mathcal{T}) \cap \mathbf{H}_0(\text{div}, \Omega) & k = 1, \\ (\mathbf{RT}_0(\mathcal{T}) \cap \mathbf{H}_0(\text{div}, \Omega)) \oplus \mathbf{RT}_1^{\text{int}}(\mathcal{T}) & k = 2, d = 3, \\ \left\{ \mathbf{v}_h \in \widetilde{\mathbf{RT}}_{k-1}^{\text{int}}(\mathcal{T}) : \text{div}(\mathbf{v}_h) \in \widehat{Q}_h^\perp \right\} & k \geq d, \end{cases}$$

where

$$\mathbf{H}_0(\text{div}, \Omega) := \{ \mathbf{v} \in \mathbf{H}(\text{div}, \Omega) : \mathbf{v} \cdot \mathbf{n} = 0 \text{ on } \partial\Omega \}.$$

Some explicit basis functions for (2.3) can be found in [25]. Later, for the construction of the reduced scheme in Section 5, for all $k \geq d$ we choose $\widehat{Q}_h = P_0^{\text{disc}}(\mathcal{T})$, which leads to a larger enrichment space \mathbf{V}_h^{R} for $k > d$ but allows for some procedure that results in a much smaller system.

Define $\mathbf{V}_h := \mathbf{V}_h^{\text{ct}} \times \mathbf{V}_h^{\text{R}}$ and $\mathbf{V}(h) := \mathbf{V} \times \mathbf{V}_h^{\text{R}}$. Throughout the paper, the superscripts ‘ct’, ‘R’, and ‘s’ are employed for $\mathbf{v} \in \mathbf{V}(h)$ in the following way: $\mathbf{v}^{\text{ct}} \in \mathbf{V}$ and $\mathbf{v}^{\text{R}} \in \mathbf{V}_h^{\text{R}}$ denote the \mathbf{H}^1 -conforming component and $\mathbf{H}(\text{div})$ -conforming component of $\mathbf{v} = (\mathbf{v}^{\text{ct}}, \mathbf{v}^{\text{R}})$, and $\mathbf{v}^{\text{s}} \in \mathbf{V} + \mathbf{V}_h^{\text{R}}$ denotes the summation of both components, i.e., $\mathbf{v}^{\text{s}} := \mathbf{v}^{\text{ct}} + \mathbf{v}^{\text{R}}$ which lives in $\mathbf{H}(\text{div}, \Omega)$ only. Moreover, any $\mathbf{v}^{\text{R}} \in \mathbf{V}_h^{\text{R}}$ can be split into

$$\mathbf{v}^{\text{R}} =: \mathbf{v}^{\text{RT}_0} + \widetilde{\mathbf{v}}^{\text{R}} = \sum_{F \in \mathcal{F}^0} \text{dof}_F(\mathbf{v}_h^{\text{RT}_0}) \psi_F + \widetilde{\mathbf{v}}^{\text{R}} \in \mathbf{RT}_0(\mathcal{T}) \oplus \widetilde{\mathbf{RT}}_{k-1}^{\text{int}}(\mathcal{T}),$$

where $\psi_F, F \in \mathcal{F}^0$, are the basis functions of $\mathbf{RT}_0(\mathcal{T}) \cap \mathbf{H}_0(\text{div}, \Omega)$, and $\text{dof}_F : \mathbf{RT}_0(\mathcal{T}) \rightarrow \mathbb{R}$ represents the degree of freedom functionals corresponding to ψ_F . Note, that for $k \geq d$, no lowest-order Raviart–Thomas functions are involved and therefore it holds $\mathbf{v}^{\text{RT}_0} = \mathbf{0}$ for all $\mathbf{v}^{\text{R}} \in \mathbf{V}_h^{\text{R}}$.

The divergence-free subspaces of \mathbf{V} , $\mathbf{V}(h)$, and \mathbf{V}_h are defined as

$$\begin{aligned}\mathbf{Z} &:= \{\mathbf{v} \in \mathbf{V} : \operatorname{div}(\mathbf{v}) = 0\}, \\ \mathbf{Z}(h) &:= \{\mathbf{v} \in \mathbf{V}(h) : \operatorname{div}(\mathbf{v}^s) = 0\}, \text{ and} \\ \mathbf{Z}_h &:= \{\mathbf{v}_h \in \mathbf{V}_h : \operatorname{div}(\mathbf{v}_h^s) = 0\}, \text{ respectively.}\end{aligned}$$

3. DISCRETIZATION OF THE NAVIER–STOKES EQUATIONS

This section discusses the extension of the enrichment strategy from the previous section for the Stokes problem to the full Navier–Stokes problem and some direct structural properties.

3.1. Discretization of the linear parts. The discrete counterpart of (1.2) applies the same bilinear forms used to discretize the stationary Stokes problem in [32, 25], i.e.,

$$a_h(\mathbf{u}, \mathbf{v}) := (\nabla \mathbf{u}^{\text{ct}}, \nabla \mathbf{v}^{\text{ct}}) - (\Delta_{\text{pw}} \mathbf{u}^{\text{ct}}, \mathbf{v}^{\text{R}}) + (\Delta_{\text{pw}} \mathbf{v}^{\text{ct}}, \mathbf{u}^{\text{R}}) + a_h^{\text{D}}(\mathbf{u}^{\text{RT}_0}, \mathbf{v}^{\text{RT}_0}),$$

where Δ_{pw} is the piecewise Laplacian operator, and

$$b(\mathbf{v}, q) := -(\operatorname{div}(\mathbf{v}^s), q),$$

and

$$a_h^{\text{D}}(\mathbf{u}^{\text{RT}_0}, \mathbf{v}^{\text{RT}_0}) := \alpha \sum_{F \in \mathcal{F}^0} \operatorname{dof}_F(\mathbf{u}_h^{\text{RT}_0}) \operatorname{dof}_F(\mathbf{v}_h^{\text{RT}_0}) (\operatorname{div} \boldsymbol{\psi}_F, \operatorname{div} \boldsymbol{\psi}_F),$$

with a positive parameter α , which is a stabilization only needed for $k < d$. Note that the coefficient matrix related to a_h^{D} is diagonal. Also recall, that $\|\cdot\|^2 := a_h(\cdot, \cdot)$ induces a seminorm $\|\cdot\|$ on $\mathbf{V}(h)$. For the time derivative, we employ

$$d_h(\mathbf{u}, \mathbf{v}) := (\mathbf{u}^s, \mathbf{v}^s).$$

3.2. Discretization of the nonlinear terms. For the discretization of the nonlinear term, which is of central importance in Navier–Stokes simulations, consider the following nonlinear forms

$$\begin{aligned}c(\widehat{\mathbf{w}}, \widehat{\mathbf{u}}, \widehat{\mathbf{v}}) &:= ((\widehat{\mathbf{w}} \cdot \nabla_h) \widehat{\mathbf{u}}, \widehat{\mathbf{v}}) \quad \text{for all } \widehat{\mathbf{w}}, \widehat{\mathbf{u}}, \widehat{\mathbf{v}} \in \mathbf{L}^2(\Omega), \\ c_h^{\text{vol}}(\mathbf{w}, \mathbf{u}, \mathbf{v}) &:= c(\mathbf{w}^s, \mathbf{u}^{\text{ct}}, \mathbf{v}^s) - c(\mathbf{w}^s, \mathbf{v}^{\text{ct}}, \mathbf{u}^{\text{R}}) \\ &= c(\mathbf{w}^s, \mathbf{u}^{\text{ct}}, \mathbf{v}^{\text{ct}}) + c(\mathbf{w}^s, \mathbf{u}^{\text{ct}}, \mathbf{v}^{\text{R}}) - c(\mathbf{w}^s, \mathbf{v}^{\text{ct}}, \mathbf{u}^{\text{R}}), \\ c_h^{\text{R}}(\mathbf{w}, \mathbf{u}, \mathbf{v}) &:= c(\mathbf{w}^s, \mathbf{u}^{\text{R}}, \mathbf{v}^{\text{R}}) - \sum_{F \in \mathcal{F}^0} \int_F (\mathbf{w}^s \cdot \mathbf{n}) \llbracket \mathbf{u}^{\text{R}} \rrbracket \cdot \{\{\mathbf{v}^{\text{R}}\}\} ds, \\ c_h^{\text{uw}}(\mathbf{w}, \mathbf{u}, \mathbf{v}) &:= \frac{1}{2} \sum_{F \in \mathcal{F}^0} \int_F |\mathbf{w}^s \cdot \mathbf{n}| \llbracket \mathbf{u}^{\text{R}} \rrbracket \cdot \llbracket \mathbf{v}^{\text{R}} \rrbracket ds,\end{aligned}$$

and

$$c_h^{\text{dG}}(\mathbf{w}, \mathbf{u}, \mathbf{v}) := c(\mathbf{w}^s, \mathbf{u}^s, \mathbf{v}^s) - \sum_{F \in \mathcal{F}^0} \int_F (\mathbf{w}^s \cdot \mathbf{n}) \llbracket \mathbf{u}^{\text{R}} \rrbracket \cdot \{\{\mathbf{v}^s\}\} ds$$

for all $\mathbf{u}, \mathbf{v}, \mathbf{w} \in \mathbf{V}(h)$, where ∇_h is the piecewise gradient operator, c_h^{vol} is inspired by [31], and c_h^{R} , c_h^{uw} (upwind stabilization) and c_h^{dG} are inspired by $\mathbf{H}(\operatorname{div})$ -conforming discontinuous Galerkin methods [22, 45].

Remark 3.1 (Relationship between c_h^{vol} , c_h^{R} and c_h^{dG}). *Note that by continuity, it holds $[[\mathbf{u}^{\text{ct}}]] = 0$. By an integration by parts, one has*

$$c_h^{\text{vol}}(\mathbf{w}, \mathbf{u}, \mathbf{v}) := c(\mathbf{w}^{\text{s}}, \mathbf{u}^{\text{ct}}, \mathbf{v}^{\text{s}}) + c(\mathbf{w}^{\text{s}}, \mathbf{u}^{\text{R}}, \mathbf{v}^{\text{ct}}) - \sum_{F \in \mathcal{F}^0} \int_F (\mathbf{w}^{\text{s}} \cdot \mathbf{n}) [[\mathbf{u}^{\text{R}}]] \{\{\mathbf{v}^{\text{ct}}\}\} ds.$$

Then it is not very hard to verify that

$$(3.1) \quad c_h^{\text{dG}}(\mathbf{w}, \mathbf{u}, \mathbf{v}) = c_h^{\text{vol}}(\mathbf{w}, \mathbf{u}, \mathbf{v}) + c_h^{\text{R}}(\mathbf{w}, \mathbf{u}, \mathbf{v}).$$

In a sense, c_h^{vol} can be regarded as an incomplete discontinuous Galerkin $\mathbf{H}(\text{div})$ -conforming formulation for nonlinear terms, which consists of volume integrals only.

3.3. Stabilizations. For the enrichment part the following two stabilizations are considered

$$\mathcal{S}_1(\mathbf{u}, \mathbf{v}) := (\partial_t \mathbf{u}^{\text{R}}, \mathbf{v}^{\text{R}}) \quad \text{and} \quad \mathcal{S}_2(\mathbf{u}, \mathbf{v}) := (h_{\mathcal{T}}^{-1} \mathbf{u}^{\text{R}}, \mathbf{v}^{\text{R}}).$$

Note that by (2.1) for $k \geq d$ the second stabilization is equivalent to

$$\mathcal{S}_2(\mathbf{u}, \mathbf{v}) \approx (h_{\mathcal{T}} \text{div} \mathbf{u}^{\text{R}}, \text{div} \mathbf{v}^{\text{R}}) = (h_{\mathcal{T}} \text{div} \mathbf{u}^{\text{ct}}, \text{div} \mathbf{v}^{\text{ct}})$$

which can be seen as a grad-div stabilization of the \mathbf{H}^1 -conforming part. However, this one here scales with h and thus is weaker than the usual one used for non-divergence-free methods like Taylor–Hood [14]. One should note that the grad-div-like stabilization here plays a different role than the grad-div stabilization for the Taylor–Hood element: the former is introduced to stabilize the nonconforming part, while the latter is used to improve the mass conservation of the discrete velocity solution. Opposite to the Taylor–Hood method, the present scheme is always pressure-robust and divergence-free.

Remark 3.2 (Connection between \mathcal{S}_1 and \mathcal{S}_2). *We use backward Euler time stepping as an example. Denote by Δt the length of the time steps. Then a corresponding discretization for \mathcal{S}_1 looks like*

$$\mathcal{S}_1^{\text{d}}(\mathbf{u}_h, \mathbf{v}_h) := \Delta t^{-1} \left((\mathbf{u}_h^{\text{R}, n+1}, \mathbf{v}_h) - (\mathbf{u}_h^{\text{R}, n}, \mathbf{v}_h) \right).$$

The $\mathbf{u}_h^{\text{R}, n}$ part should be shifted to the right-hand side in the computation. If we ignore the right-hand side part and suppose $\Delta t \approx h$, one can see that there is some similarity between \mathcal{S}_1 and \mathcal{S}_2 .

3.4. Discretization schemes. This paper investigates two discretization variants for (1.1) or (1.2).

The first one employs the DG upwind discretization for the nonlinear term: Find $(\mathbf{u}_h, p_h) : (0, T] \rightarrow \mathbf{V}_h \times Q_h$ such that

$$(3.2) \quad \begin{aligned} d_h(\partial_t \mathbf{u}_h, \mathbf{v}_h) + c_h^{\text{dG}}(\mathbf{u}_h, \mathbf{u}_h, \mathbf{v}_h) + c_h^{\text{uw}}(\mathbf{u}_h, \mathbf{u}_h, \mathbf{v}_h) \\ + \nu a_h(\mathbf{u}_h, \mathbf{v}_h) + b(\mathbf{v}_h, p_h) = (\mathbf{f}, \mathbf{v}_h^{\text{s}}) \quad \text{for all } \mathbf{v}_h \in \mathbf{V}_h, \\ b(\mathbf{u}_h, q_h) = 0 \quad \text{for all } q_h \in Q_h, \end{aligned}$$

and $\mathbf{u}_h(0) = \mathbf{u}_h^0$ with \mathbf{u}_h^0 being some suitable approximation of $(\mathbf{u}^0, \mathbf{0})$.

The second discretization employs c_h^{vol} plus one of the two stabilizations $\mathcal{S} \in \{\mathcal{S}_1, \mathcal{S}_2\}$: Find $(\mathbf{u}_h, p_h) : (0, T] \rightarrow \mathbf{V}_h \times Q_h$ such that

$$(3.3) \quad \begin{aligned} d_h(\partial_t \mathbf{u}_h, \mathbf{v}_h) + c_h^{\text{vol}}(\mathbf{u}_h, \mathbf{u}_h, \mathbf{v}_h) + \gamma \mathcal{S}(\mathbf{u}_h, \mathbf{v}_h) \\ + \nu a_h(\mathbf{u}_h, \mathbf{v}_h) + b(\mathbf{v}_h, p_h) = (\mathbf{f}, \mathbf{v}_h^{\text{s}}) \quad \text{for all } \mathbf{v}_h \in \mathbf{V}_h, \\ b(\mathbf{u}_h, q_h) = 0 \quad \text{for all } q_h \in Q_h, \end{aligned}$$

and also $\mathbf{u}_h(0) = \mathbf{u}_h^0$ with \mathbf{u}_h^0 being some suitable approximation of $(\mathbf{u}^0, \mathbf{0})$. Here, γ denotes some parameter to scale the stabilization.

By removing the Lagrange multiplier and seeking the solution directly in the space of divergence-free functions, both systems (3.2) and (3.3) seek $\mathbf{u}_h : (0, T] \rightarrow \mathbf{Z}_h$ with $\mathbf{u}_h(0) = \mathbf{u}_h^0$ such that

$$(3.4) \quad d_h(\partial_t \mathbf{u}_h, \mathbf{v}_h) + c_h^{\text{dG}}(\mathbf{u}_h, \mathbf{u}_h, \mathbf{v}_h) + c_h^{\text{uw}}(\mathbf{u}_h, \mathbf{u}_h, \mathbf{v}_h) + \nu a_h(\mathbf{u}_h, \mathbf{v}_h) = (\mathbf{f}, \mathbf{v}_h^{\text{s}})$$

and

$$(3.5) \quad d_h(\partial_t \mathbf{u}_h, \mathbf{v}_h) + c_h^{\text{vol}}(\mathbf{u}_h, \mathbf{u}_h, \mathbf{v}_h) + \gamma \mathcal{S}(\mathbf{u}_h, \mathbf{v}_h) + \nu a_h(\mathbf{u}_h, \mathbf{v}_h) = (\mathbf{f}, \mathbf{v}_h^{\text{s}})$$

for all $\mathbf{v}_h \in \mathbf{Z}_h$, respectively.

3.5. EMA-conservation. It has been shown in the paper [11, Theorem 4] that the upwind DG formulation ($c_h^{\text{dG}} + c_h^{\text{uw}}$) is momentum-conserving and angular momentum-conserving under the assumption that all data is compactly supported (see the assumption in Lemma 3.5 below). There it is also proven that the scheme with upwind DG formulation is energy-stable. Although their analysis is based on the DG formulation for the diffusion term, there is no essential difference on EMA-conservation for our method. Thus this subsection only discusses this aspect for the other scheme (3.3).

Lemma 3.3. *For any $(\mathbf{u}, \mathbf{v}, \mathbf{w}) \in \mathbf{V}(h) \times \mathbf{V}(h) \times \mathbf{Z}(h)$, the trilinear form c_h fulfills*

$$(3.6) \quad c_h^{\text{vol}}(\mathbf{w}, \mathbf{u}, \mathbf{v}) = -c_h^{\text{vol}}(\mathbf{w}, \mathbf{v}, \mathbf{u}).$$

Proof. The above identity follows immediately from $((\mathbf{w}^{\text{s}} \cdot \nabla) \mathbf{u}^{\text{ct}}, \mathbf{v}^{\text{ct}}) = -((\mathbf{w}^{\text{s}} \cdot \nabla) \mathbf{v}^{\text{ct}}, \mathbf{u}^{\text{ct}})$ and the definition of c_h^{vol} . \square

Lemma 3.3 implies that

$$(3.7) \quad c_h^{\text{vol}}(\mathbf{w}, \mathbf{v}, \mathbf{v}) = 0 \quad \text{for all } \mathbf{v} \in \mathbf{V}(h), \mathbf{w} \in \mathbf{Z}(h).$$

The quantities under consideration are the kinetic energy E , linear momentum M and angular momentum $M_{\mathbf{x}}$ defined by

$$\begin{aligned} E : \mathbf{Z}(h) &\rightarrow \mathbb{R}, & E(\mathbf{u}) &:= \frac{1}{2} d_h(\mathbf{u}, \mathbf{u}) = \frac{1}{2} \int_{\Omega} |\mathbf{u}^{\text{s}}|^2 \, d\mathbf{x}, \\ M : \mathbf{Z}(h) &\rightarrow \mathbb{R}^d, & M(\mathbf{u}) &:= \int_{\Omega} \mathbf{u}^{\text{s}} \, d\mathbf{x}, \\ M_{\mathbf{x}} : \mathbf{Z}(h) &\rightarrow \mathbb{R}^3, & M_{\mathbf{x}}(\mathbf{u}) &:= \int_{\Omega} \mathbf{u}^{\text{s}} \times \mathbf{x} \, d\mathbf{x}, \end{aligned}$$

for any $\mathbf{u} \in \mathbf{Z}(h)$.

Lemma 3.4. *Let \mathbf{u}_h be the solution of (3.3). It holds*

$$E(\mathbf{u}_h) + \mathcal{S}(\mathbf{u}_h, \mathbf{u}_h) + \nu \|\mathbf{u}_h\| = (\mathbf{f}, \mathbf{u}_h).$$

Proof. That is a direct consequence of testing (3.3) with $\mathbf{v}_h = \mathbf{u}_h$ and the skew-symmetry of c_h^{vol} . \square

Lemma 3.5. *Let \mathbf{u}_h be the solution of (3.3). Assume that \mathbf{u}_h , p_h and \mathbf{f} are compactly supported on a subdomain Ω_{ω} such that there exists an operator $\chi : \mathbf{L}^2(\Omega) \rightarrow \mathbf{V}(h)$ satisfying $\chi(\mathbf{g})|_{\Omega_{\omega}} = \mathbf{g}$ for $\mathbf{g} = \mathbf{e}_i, \mathbf{x} \times \mathbf{e}_i, i = 1, \dots, d$, with $\mathbf{e}_i \in \mathbb{R}^d$ being the unit vector with respect to the i -th component. Then, the following identities are satisfied:*

$$\frac{d}{dt} M(\mathbf{u}_h) = \int_{\Omega} \mathbf{f} \, d\mathbf{x}, \quad \frac{d}{dt} M_{\mathbf{x}}(\mathbf{u}_h) = \int_{\Omega} \mathbf{f} \times \mathbf{x} \, d\mathbf{x}.$$

Proof. The proof of this lemma is very similar to the proof of [31, Theorem 2.2]. \square

Lemma 3.4 shows that the energy is conserved in some discrete sense that takes into account also the stabilization. Lemma 3.5 shows that the linear momentum and angular momentum are conserved exactly.

4. PRESSURE ROBUST AND CONVECTION-ROBUST ERROR ESTIMATE

The section investigates a priori error estimates and shows that pressure-robustness and convection-robustness can be attained for both suggested schemes.

4.1. Approximation properties and stability of a projection operator. In this subsection a projection operator is designed, which will be used in the error analysis of the proposed schemes. For any $\mathbf{v} \in \mathbf{V}$ and $k \geq d$, we define the Stokes projection operator

$$\widehat{\Pi}_h^{\text{St}} : \mathbf{Z} \rightarrow \widehat{\mathbf{Z}}_h := \{\mathbf{v}_h \in \mathbf{V}_h^{\text{ct}} : b(\mathbf{v}_h, q_h) = 0 \text{ for all } q_h \in \widehat{Q}_h\}$$

with the inf-sup stable sub-pair $\mathbf{V}_h^{\text{ct}} \times \widehat{Q}_h \subseteq \mathbf{V}_h^{\text{ct}} \times Q_h$ mentioned in Section 2.2 by seeking $\widehat{\Pi}_h^{\text{St}} \mathbf{v} \in \widehat{\mathbf{Z}}_h$ such that

$$\left(\nabla \widehat{\Pi}_h^{\text{St}} \mathbf{v}, \nabla \mathbf{w} \right) = (\nabla \mathbf{v}, \nabla \mathbf{w}) \quad \text{for all } \mathbf{w} \in \widehat{\mathbf{Z}}_h.$$

According to standard Stokes theory such as [26], it satisfies

$$(4.1) \quad \|\mathbf{v} - \widehat{\Pi}_h^{\text{St}} \mathbf{v}\| + h \|\nabla(\mathbf{v} - \widehat{\Pi}_h^{\text{St}} \mathbf{v})\| \lesssim h \inf_{\mathbf{w} \in \mathbf{V}_h^{\text{ct}}} \|\nabla(\mathbf{v} - \mathbf{w})\|.$$

In case $k < d$, where \widehat{Q}_h is chosen to be the zero space, $\widehat{\Pi}_h^{\text{St}} : \mathbf{Z} \rightarrow \mathbf{V}_h^{\text{ct}}$ is defined as a quasi-interpolation operator [7, Section 4.8], which satisfies

$$(4.2) \quad \|\mathbf{v} - \widehat{\Pi}_h^{\text{St}} \mathbf{v}\|_{\mathbf{L}^p(T)} + h_T \|\nabla(\mathbf{v} - \widehat{\Pi}_h^{\text{St}} \mathbf{v})\|_{\mathbf{L}^p(T)} \lesssim h_T^r |\mathbf{v}|_{\mathbf{W}^{r,p}(\omega(T))}, \quad p = 2, \infty,$$

for all $T \in \mathcal{T}$, $1 \leq r \leq k$, with $\omega(T)$ being a suitable neighborhood containing T .

Assumption 4.1. For any $\mathbf{v} \in \mathbf{W}^{1,\infty}(\Omega) \cap \mathbf{Z}$, we assume that the following estimate holds:

$$(4.3) \quad \|\mathbf{v} - \widehat{\Pi}_h^{\text{St}} \mathbf{v}\|_{\mathbf{L}^\infty} + h \|\nabla \widehat{\Pi}_h^{\text{St}} \mathbf{v}\|_{\mathbf{L}^\infty} \lesssim h \|\nabla \mathbf{v}\|_{\mathbf{L}^\infty}.$$

Remark 4.2. For $k < d$, (4.3) can be derived from (4.2) by choosing $r = 1$. For $k \geq d$, the bound for $\|\nabla \widehat{\Pi}_h^{\text{St}} \mathbf{v}\|_{\mathbf{L}^\infty}$ was shown in [17] in case that Ω is convex and \mathcal{T} is quasi-uniform. A similar assumption can be also found in [45, 31].

Next, define $\Pi_h^{\text{St}} : \mathbf{Z} \rightarrow \mathbf{Z}_h$ as

$$(4.4) \quad \Pi_h^{\text{St}} \mathbf{v} := \begin{cases} \left(\widehat{\Pi}_h^{\text{St}} \mathbf{v}, \mathcal{R} \widehat{\mathbf{v}} \right) & \text{for } k \geq d, \\ \left(\widehat{\Pi}_h^{\text{St}} \mathbf{v}, (\Pi^{\text{RT}_0} + \mathcal{R}) \widehat{\mathbf{v}} \right) & \text{for } k < d, \end{cases} \quad \text{with } \widehat{\mathbf{v}} := \mathbf{v} - \widehat{\Pi}_h^{\text{St}} \mathbf{v},$$

where Π^{RT_0} is the usual interpolation operator for \mathbf{RT}_0 , and \mathcal{R} is the div- L^2 projection onto the $\mathbf{H}(\text{div})$ cell bubble space part of \mathbf{V}_h^{R} with respect to the $(\text{div} \bullet, \text{div} \bullet)$ inner product and therefore it satisfies

$$(4.5) \quad \|\text{div}(\mathcal{R} \widehat{\mathbf{v}})\|_{L^2(T)} \leq \|\text{div}(\widehat{\mathbf{v}})\|_{L^2(T)} = \|\text{div}(\widehat{\Pi}_h^{\text{St}} \mathbf{v})\|_{L^2(T)}.$$

Note, that this resembles the structure of the Fortin interpolator in [25, Lemma 4.1] and by design it holds $\Pi_h^{\text{St}} \mathbf{v} \in \mathbf{Z}_h$ for any $\mathbf{v} \in \mathbf{Z}$.

Lemma 4.3. For $\mathbf{v} \in \mathbf{Z}$, Π_h^{St} satisfies

$$\|\mathbf{v} - (\Pi_h^{\text{St}} \mathbf{v})^s\| + h \|\nabla(\mathbf{v} - (\Pi_h^{\text{St}} \mathbf{v})^{\text{ct}})\| \lesssim h \inf_{\mathbf{w}^{\text{ct}} \in \mathbf{V}_h^{\text{ct}}} \|\nabla(\mathbf{v} - \mathbf{w}^{\text{ct}})\|$$

for $k \geq d$, and for $k < d$,

$$\|\mathbf{v} - (\Pi_h^{\text{St}} \mathbf{v})^s\| + h \|\nabla(\mathbf{v} - (\Pi_h^{\text{St}} \mathbf{v})^{\text{ct}})\| + h \|h_{\mathcal{T}}^{-1} (\Pi_h^{\text{St}} \mathbf{v})^{\text{R}}\| \lesssim h^r |\mathbf{v}|_{\mathbf{H}^r},$$

with $1 \leq r \leq k$. Additionally, under Assumption 4.1, we further have

$$(4.6) \quad \|\mathbf{v} - (\Pi_h^{\text{St}} \mathbf{v})^s\|_{\mathbf{L}^\infty} \lesssim h \|\nabla \mathbf{v}\|_{\mathbf{L}^\infty},$$

and

$$(4.7) \quad \|\nabla(\Pi_h^{\text{St}} \mathbf{v})^{\text{ct}}\|_{\mathbf{L}^\infty} + \|h_{\mathcal{T}}^{-1} (\Pi_h^{\text{St}} \mathbf{v})^{\text{R}}\|_{\mathbf{L}^\infty} \lesssim \|\nabla \mathbf{v}\|_{\mathbf{L}^\infty}.$$

Proof. Due to (4.1) and (4.2), it suffices to show the \mathbf{L}^2 -bound and \mathbf{L}^∞ -bound for the \mathbf{V}_h^{R} -part of (4.4). Consider an arbitrary $\mathbf{v} \in \mathbf{Z}$ with sufficient regularity. We prove the \mathbf{L}^2 -bound first. For the \mathbf{RT}_0 part, from the approximation property of Π^{RT_0} [6, Proposition 2.5.1]

$$\|\mathbf{w} - \Pi^{\text{RT}_0} \mathbf{w}\|_{\mathbf{L}^2(T)} \lesssim h_T \|\nabla \mathbf{w}\|_{\mathbf{L}^2(T)}$$

and the triangle inequality, we have

$$(4.8) \quad \|\Pi^{\text{RT}_0} \mathbf{w}\|_{\mathbf{L}^2(T)} \lesssim \|\mathbf{w}\|_{\mathbf{L}^2(T)} + h_T \|\nabla \mathbf{w}\|_{\mathbf{L}^2(T)}$$

for all $\mathbf{w} \in \mathbf{H}^1(T)$, which, together with (4.2), implies that

$$\|\Pi^{\text{RT}_0} \hat{\mathbf{v}}\|_{\mathbf{L}^2(T)} \lesssim \|\hat{\mathbf{v}}\|_{\mathbf{L}^2(T)} + h_T \|\nabla \hat{\mathbf{v}}\|_{\mathbf{L}^2(T)} \lesssim h_T^r |\mathbf{v}|_{\mathbf{H}^r(\omega(T))}.$$

For the higher order Raviart–Thomas part, according to Lemma 2.1 and (4.5) one has

$$h_T^{-1} \|\mathcal{R} \hat{\mathbf{v}}\|_{\mathbf{L}^2(T)} \lesssim \|\text{div}(\mathcal{R} \hat{\mathbf{v}})\|_{\mathbf{L}^2(T)} \leq \|\text{div}(\hat{\mathbf{v}})\|_{\mathbf{L}^2(T)} \leq \|\nabla(\hat{\mathbf{v}})\|_{\mathbf{L}^2(T)}.$$

Then it follows from summation over $T \in \mathcal{T}$, (4.1), (4.2), and the fact that $(\Pi_h^{\text{St}} \mathbf{v})^{\text{R}} = \mathcal{R} \hat{\mathbf{v}}$ or $(\Pi_h^{\text{St}} \mathbf{v})^{\text{R}} = (\Pi^{\text{RT}_0} + \mathcal{R}) \hat{\mathbf{v}}$ that

$$\|(\Pi_h^{\text{St}} \mathbf{v})^{\text{R}}\| + h \|h_{\mathcal{T}}^{-1} (\Pi_h^{\text{St}} \mathbf{v})^{\text{R}}\| \lesssim \begin{cases} h \inf_{\mathbf{w}^{\text{ct}} \in \mathbf{V}_h^{\text{ct}}} \|\nabla(\mathbf{v} - \mathbf{w}^{\text{ct}})\| & \text{for } k \geq d, \\ h^r |\mathbf{v}|_{\mathbf{H}^r} & \text{for } k < d. \end{cases}$$

Let us consider the \mathbf{L}^∞ -bound. For $k \geq d$, no \mathbf{RT}_0 functions are involved, and inverse inequalities, Lemma 2.1, and (4.3) yield

$$\begin{aligned} h_T^{-1} \|(\Pi_h^{\text{St}} \mathbf{v})^{\text{R}}\|_{\mathbf{L}^\infty(T)} &= h_T^{-1} \|\mathcal{R} \hat{\mathbf{v}}\|_{\mathbf{L}^\infty(T)} \\ &\lesssim h_T^{-1-d/2} \|\mathcal{R} \hat{\mathbf{v}}\|_{\mathbf{L}^2(T)} \\ &\lesssim h_T^{-d/2} \|\text{div}(\mathcal{R} \hat{\mathbf{v}})\|_{\mathbf{L}^2(T)} \\ &= h_T^{-d/2} \|\text{div}(\hat{\Pi}_h^{\text{St}} \mathbf{v})\|_{\mathbf{L}^2(T)} \\ &\lesssim \|\text{div}(\hat{\Pi}_h^{\text{St}} \mathbf{v})\|_{\mathbf{L}^\infty(T)} \\ &\leq \|\nabla \hat{\Pi}_h^{\text{St}} \mathbf{v}\|_{\mathbf{L}^\infty(T)} \lesssim \|\nabla \mathbf{v}\|_{\mathbf{L}^\infty(T)}, \end{aligned}$$

where we also use the inequality $\|\mathbf{w}\|_{\mathbf{L}^2(T)}^2 \leq h_T^{d/2} \|\mathbf{w}\|_{\mathbf{L}^\infty(T)}$ derived from

$$\begin{aligned} \|\mathbf{w}\|_{\mathbf{L}^2(T)}^2 &\leq \|\mathbf{w}\|_{\mathbf{L}^1(T)} \|\mathbf{w}\|_{\mathbf{L}^\infty(T)} \leq \|1\|_{\mathbf{L}^2(T)} \|\mathbf{w}\|_{\mathbf{L}^2(T)} \|\mathbf{w}\|_{\mathbf{L}^\infty(T)} \\ &\leq h_T^{d/2} \|\mathbf{w}\|_{\mathbf{L}^2(T)} \|\mathbf{w}\|_{\mathbf{L}^\infty(T)} \end{aligned}$$

for all $\mathbf{w} \in \mathbf{L}^\infty(T)$. For $k < d$, $\mathcal{R}\hat{\mathbf{w}}$ can be bounded in a very similar way. For \mathbf{RT}_0 part, it holds from inverse inequalities, (4.8), and (4.2) that

$$\begin{aligned} h_T^{-1} \|\Pi^{\mathbf{RT}_0} \hat{\mathbf{v}}\|_{\mathbf{L}^\infty(T)} &\lesssim h_T^{-1-d/2} \|\Pi^{\mathbf{RT}_0} \hat{\mathbf{v}}\|_{\mathbf{L}^2(T)} \\ &\lesssim h_T^{-d/2} (h_T^{-1} \|\hat{\mathbf{v}}\|_{\mathbf{L}^2(T)} + \|\nabla \hat{\mathbf{v}}\|_{\mathbf{L}^2(T)}) \\ &\lesssim h_T^{-d/2} \|\nabla \mathbf{v}\|_{\mathbf{L}^2(\omega(T))} \\ &\lesssim \|\nabla \mathbf{v}\|_{\mathbf{L}^\infty(\omega(T))}. \end{aligned}$$

Since, this holds for all $T \in \mathcal{T}$, one arrives at

$$\|h_{\mathcal{T}}^{-1} \left(\Pi_h^{\text{St}} \mathbf{v} \right)^{\mathbf{R}}\|_{\mathbf{L}^\infty} \lesssim \|\nabla \mathbf{v}\|_{\mathbf{L}^\infty}.$$

This concludes the proof. \square

In what follows we will assume $\mathbf{u}(t) \in \mathbf{W}^{1,\infty}(\Omega)$ for all $t \leq T$. Note, that this also guarantees $\mathbf{u}(t) \in \mathbf{C}^0(\bar{\Omega})$ according to the Sobolev imbedding theorem [18].

4.2. Analysis of the upwind scheme (3.2). To shorten the notation, we define $c_h := c_h^{\text{dG}} + c_h^{\text{uw}}$. Let \mathbf{u} be the solution of (1.2) and $\tilde{\mathbf{u}} := (\mathbf{u}, \mathbf{0}) \in \mathbf{Z}(h)$ be its representation in \mathbf{Z}_h . Due to the exact incompressibility of the functions in \mathbf{Z}_h , one can check that $\tilde{\mathbf{u}}$ fulfills the identity

$$(4.9) \quad d_h(\partial_t \tilde{\mathbf{u}}, \mathbf{v}_h) + c_h(\tilde{\mathbf{u}}, \tilde{\mathbf{u}}, \mathbf{v}_h) + \nu a_h(\tilde{\mathbf{u}}, \mathbf{v}_h) = (\mathbf{f}, \mathbf{v}_h^{\text{s}}) \quad \text{for all } \mathbf{v}_h \in \mathbf{Z}_h.$$

Consider the decomposition of the error $\mathbf{e}_h := \tilde{\mathbf{u}} - \mathbf{u}_h = \boldsymbol{\eta} + \boldsymbol{\phi}_h$ into

$$(4.10) \quad \boldsymbol{\eta} := \tilde{\mathbf{u}} - \Pi_h^{\text{St}} \mathbf{u} \quad \text{and} \quad \boldsymbol{\phi}_h := \Pi_h^{\text{St}} \mathbf{u} - \mathbf{u}_h.$$

Subtracting (3.4) from (4.9) yields, for all $\mathbf{v}_h \in \mathbf{Z}_h$,

$$(4.11) \quad \begin{aligned} d_h(\partial_t \boldsymbol{\phi}_h, \mathbf{v}_h) + \nu a_h(\boldsymbol{\phi}_h, \mathbf{v}_h) &= -d_h(\boldsymbol{\eta}_t, \mathbf{v}_h) - \nu a_h(\boldsymbol{\eta}, \mathbf{v}_h) \\ &\quad - c_h(\tilde{\mathbf{u}}, \tilde{\mathbf{u}}, \mathbf{v}_h) + c_h(\mathbf{u}_h, \mathbf{u}_h, \mathbf{v}_h). \end{aligned}$$

The error equation (4.11) is used to estimate the velocity error bound below.

Moreover, for any \mathbf{w}_h , one can define the upwind semi-norm

$$|\mathbf{v}_h|_{\mathbf{w}_h, \text{uw}} := c_h^{\text{uw}}(\mathbf{w}_h, \mathbf{v}_h, \mathbf{v}_h)$$

and bound the error of the convection terms by the following lemma.

Lemma 4.4 ([45]). *Let \mathbf{u} be the solution of (1.2) and \mathbf{u}_h be the solution of (3.4). Assume that $\mathbf{u} \in L^2((0, T]; \mathbf{W}^{1,\infty}(\Omega))$. Under Assumption 4.1 it holds that*

$$(4.12) \quad \begin{aligned} |c_h(\tilde{\mathbf{u}}, \tilde{\mathbf{u}}, \boldsymbol{\phi}_h) - c_h(\mathbf{u}_h, \mathbf{u}_h, \boldsymbol{\phi}_h)| &\leq -|\boldsymbol{\phi}_h|_{\mathbf{u}_h, \text{uw}}^2 \\ &\quad + C[\|\mathbf{u}\|_{\mathbf{L}^\infty} \|\nabla_h \boldsymbol{\eta}\|^2 + (1 + h^{-2}) \|\nabla \mathbf{u}\|_{\mathbf{L}^\infty} \|\boldsymbol{\eta}^{\text{s}}\|^2] + C\|\mathbf{u}\|_{\mathbf{W}^{1,\infty}} \|\boldsymbol{\phi}_h\|^2. \end{aligned}$$

Proof. This estimate follows from taking $\varepsilon_1 = \varepsilon_2 = 1$ and $\varepsilon_3 = \varepsilon_4 = h$ in [45, Lemma 5.5]. \square

Theorem 4.5. *Let \mathbf{u} be the solution of (1.2) and \mathbf{u}_h be the solution of (3.4). Assume that $\mathbf{u} \in L^2((0, T]; \mathbf{W}^{1, \infty}(\Omega))$, $\mathbf{u}_h^0 = \Pi_h^{\text{St}} \mathbf{u}(0)$, and Assumption 4.1 holds. The following estimate holds with $K(\mathbf{u}, T) := 1 + C\|\mathbf{u}\|_{L^1((0, T]; \mathbf{W}^{1, \infty}(\Omega))}$:*

$$(4.13) \quad E(\mathbf{e}_h(T)) + \int_0^T \left(\nu \|\mathbf{e}_h\|^2 + |\mathbf{e}_h|_{\mathbf{u}_h, \mathbf{u}_w}^2 \right) dt \\ \leq E(\boldsymbol{\eta}(T)) + \int_0^T \left(\nu \|\boldsymbol{\eta}\|^2 + |\boldsymbol{\eta}|_{\mathbf{u}_h, \mathbf{u}_w}^2 \right) dt + e^{K(\mathbf{u}, T)} \int_0^T \left\{ TE(\partial_t \boldsymbol{\eta}) \right. \\ \left. + C\nu \|\boldsymbol{\eta}\|^2 + C[\|\mathbf{u}\|_{L^\infty} \|\nabla_h \boldsymbol{\eta}\|^2 + (1 + h^{-2}) \|\nabla \mathbf{u}\|_{L^\infty} \|\boldsymbol{\eta}^s\|^2] \right\} dt.$$

Proof. Taking $\mathbf{v}_h = \boldsymbol{\phi}_h$ in (4.11) gives

$$(4.14) \quad \frac{d}{dt} E(\boldsymbol{\phi}_h) + \nu \|\boldsymbol{\phi}_h\|^2 = -d_h(\partial_t \boldsymbol{\eta}, \boldsymbol{\phi}_h) - \nu a_h(\boldsymbol{\eta}, \boldsymbol{\phi}_h) - c_h(\tilde{\mathbf{u}}, \tilde{\mathbf{u}}, \boldsymbol{\phi}_h) + c_h(\mathbf{u}_h, \mathbf{u}_h, \boldsymbol{\phi}_h).$$

Note that

$$(4.15) \quad |d_h(\partial_t \boldsymbol{\eta}, \boldsymbol{\phi}_h)| \leq TE(\partial_t \boldsymbol{\eta}) + \frac{1}{T} E(\boldsymbol{\phi}_h)$$

and

$$(4.16) \quad \nu |a_h(\boldsymbol{\eta}, \boldsymbol{\phi}_h)| \leq C\nu \|\boldsymbol{\eta}\|^2 + \frac{\nu}{2} \|\boldsymbol{\phi}_h\|^2.$$

A combination of (4.14), (4.15), (4.16), and (4.12) gives

$$\frac{d}{dt} E(\boldsymbol{\phi}_h) + \frac{\nu}{2} \|\boldsymbol{\phi}_h\|^2 + |\boldsymbol{\phi}_h|_{\mathbf{w}_h, \mathbf{u}_w}^2 \leq TE(\partial_t \boldsymbol{\eta}) + \frac{1}{T} E(\boldsymbol{\phi}_h) + C\nu \|\boldsymbol{\eta}\|^2 \\ + C[\|\mathbf{u}\|_{L^\infty} \|\nabla_h \boldsymbol{\eta}\|^2 + (1 + h^{-2}) \|\nabla \mathbf{u}\|_{L^\infty} \|\boldsymbol{\eta}^s\|^2] + C\|\mathbf{u}\|_{\mathbf{W}^{1, \infty}} \|\boldsymbol{\phi}_h\|^2.$$

The Gronwall inequality, integration over $(0, T]$, and choosing $\mathbf{u}_h^0 = \Pi_h^{\text{St}} \mathbf{u}(0)$ lead to

$$E(\boldsymbol{\phi}_h(T)) + \int_0^T \left(\frac{\nu}{2} \|\boldsymbol{\phi}_h\|^2 + |\boldsymbol{\phi}_h|_{\mathbf{w}_h, \mathbf{u}_w}^2 \right) dt \leq e^{K(\mathbf{u}, T)} \int_0^T \left\{ TE(\partial_t \boldsymbol{\eta}) \right. \\ \left. + C\nu \|\boldsymbol{\eta}\|^2 + C[\|\mathbf{u}\|_{L^\infty} \|\nabla_h \boldsymbol{\eta}\|^2 + (1 + h^{-2}) \|\nabla \mathbf{u}\|_{L^\infty} \|\boldsymbol{\eta}^s\|^2] \right\} dt.$$

Then (4.13) follows immediately. This completes the proof. \square

4.3. Analysis of the scheme (3.3). For the scheme (3.3), the error decomposition (4.10) this time leads to the error equation

$$(4.17) \quad d_h(\partial_t \boldsymbol{\phi}_h, \mathbf{v}_h) + \nu a_h(\boldsymbol{\phi}_h, \mathbf{v}_h) + \gamma \mathcal{S}(\boldsymbol{\phi}_h, \mathbf{v}_h) = -d_h(\boldsymbol{\eta}_t, \mathbf{v}_h) - \nu a_h(\boldsymbol{\eta}, \mathbf{v}_h) \\ - \gamma \mathcal{S}(\boldsymbol{\eta}, \mathbf{v}_h) - c_h^{\text{vol}}(\tilde{\mathbf{u}}, \tilde{\mathbf{u}}, \mathbf{v}_h) + c_h^{\text{vol}}(\mathbf{u}_h, \mathbf{u}_h, \mathbf{v}_h) \text{ for all } \mathbf{v}_h \in \mathbf{Z}_h.$$

Taking $\mathbf{v}_h = \boldsymbol{\phi}_h$ in (4.17) one obtains

$$(4.18) \quad \frac{d}{dt} E(\boldsymbol{\phi}_h) + \nu \|\boldsymbol{\phi}_h\|^2 + \gamma \mathcal{S}(\boldsymbol{\phi}_h, \boldsymbol{\phi}_h) = -d_h(\boldsymbol{\eta}_t, \boldsymbol{\phi}_h) - \nu a_h(\boldsymbol{\eta}, \boldsymbol{\phi}_h) \\ - \gamma \mathcal{S}(\boldsymbol{\eta}, \boldsymbol{\phi}_h) - c_h^{\text{vol}}(\tilde{\mathbf{u}}, \tilde{\mathbf{u}}, \boldsymbol{\phi}_h) + c_h^{\text{vol}}(\mathbf{u}_h, \mathbf{u}_h, \boldsymbol{\phi}_h).$$

According to (3.1) and the fact that $c_h^{\text{vol}}(\tilde{\mathbf{u}}, \tilde{\mathbf{u}}, \mathbf{v}_h) = c_h^{\text{dG}}(\tilde{\mathbf{u}}, \tilde{\mathbf{u}}, \mathbf{v}_h)$, we split the difference of the nonlinear terms as

$$(4.19) \quad c_h^{\text{vol}}(\tilde{\mathbf{u}}, \tilde{\mathbf{u}}, \mathbf{v}_h) - c_h^{\text{vol}}(\mathbf{u}_h, \mathbf{u}_h, \mathbf{v}_h) = c_h^{\text{vol}}(\tilde{\mathbf{u}}, \tilde{\mathbf{u}}, \mathbf{v}_h) - c_h^{\text{dG}}(\mathbf{u}_h, \mathbf{u}_h, \mathbf{v}_h) + c_h^{\text{R}}(\mathbf{u}_h, \mathbf{u}_h, \mathbf{v}_h) \\ = c_h^{\text{dG}}(\tilde{\mathbf{u}}, \tilde{\mathbf{u}}, \mathbf{v}_h) - c_h^{\text{dG}}(\mathbf{u}_h, \mathbf{u}_h, \mathbf{v}_h) + c_h^{\text{R}}(\mathbf{u}_h, \mathbf{u}_h, \mathbf{v}_h).$$

Lemma 4.6 ([45]). *Let \mathbf{u} be the solution of (1.2) and \mathbf{u}_h be the solution of (3.5). Assume that $\mathbf{u} \in L^2((0, T]; \mathbf{W}^{1, \infty}(\Omega))$. Under Assumption 4.1 it holds that*

$$(4.20) \quad |c_h^{\text{dG}}(\tilde{\mathbf{u}}, \tilde{\mathbf{u}}, \phi_h) - c_h^{\text{dG}}(\mathbf{u}_h, \mathbf{u}_h, \phi_h)| \leq C[\|\mathbf{u}\|_{\mathbf{L}^\infty} \|\nabla_h \boldsymbol{\eta}^s\|^2 + (1 + h^{-2}) \|\nabla \mathbf{u}\|_{\mathbf{L}^\infty} \|\boldsymbol{\eta}^s\|^2] + C\|\mathbf{u}\|_{\mathbf{W}^{1, \infty}} \|\phi_h^s\|^2.$$

Proof. The proof is similar to that of Lemma 4.4, but without the estimate of the upwind term in [45, Lemma 5.5]. \square

Lemma 4.7. *With the same assumption as in Lemma 4.6, it holds*

$$(4.21) \quad |c_h^{\text{R}}(\mathbf{u}_h, \mathbf{u}_h, \phi_h)| \lesssim \|\mathbf{u}\|_{\mathbf{L}^\infty} \|h_{\mathcal{T}}^{-1} \boldsymbol{\eta}^{\text{R}}\| \|\phi_h^{\text{R}}\| + \|\nabla \mathbf{u}\|_{\mathbf{L}^\infty} (\|\boldsymbol{\eta}^s\| + \|\phi_h^s\|) \|\phi_h^{\text{R}}\|.$$

Proof. Note that $\tilde{\mathbf{u}}^{\text{R}} = \mathbf{0}$ and $c_h^{\text{R}}(\mathbf{w}_h, \bullet, \bullet)$ is also skew-symmetric as long as $\text{div}(\mathbf{w}_h^s) = 0$. We have

$$\begin{aligned} -c_h^{\text{R}}(\mathbf{u}_h, \mathbf{u}_h, \phi_h) &= c_h^{\text{R}}(\tilde{\mathbf{u}}, \tilde{\mathbf{u}}, \phi_h) - c_h^{\text{R}}(\mathbf{u}_h, \mathbf{u}_h, \phi_h) \\ &= c_h^{\text{R}}(\tilde{\mathbf{u}}, \boldsymbol{\eta}, \phi_h) + c_h^{\text{R}}(\tilde{\mathbf{u}}, \Pi_h^{\text{St}} \mathbf{u}, \phi_h) - c_h^{\text{R}}(\mathbf{u}_h, \mathbf{u}_h, \phi_h) \\ &= c_h^{\text{R}}(\tilde{\mathbf{u}}, \boldsymbol{\eta}, \phi_h) + c_h^{\text{R}}(\mathbf{e}_h, \Pi_h^{\text{St}} \mathbf{u}, \phi_h) + c_h^{\text{R}}(\mathbf{u}_h, \phi_h, \phi_h) \\ &= c_h^{\text{R}}(\tilde{\mathbf{u}}, \boldsymbol{\eta}, \phi_h) + c_h^{\text{R}}(\boldsymbol{\eta}, \Pi_h^{\text{St}} \mathbf{u}, \phi_h) + c_h^{\text{R}}(\phi_h, \Pi_h^{\text{St}} \mathbf{u}, \phi_h), \end{aligned}$$

where the final equality follows from the fact $c_h^{\text{R}}(\mathbf{u}_h, \phi_h, \phi_h) = 0$. By the Hölder inequality, trace inequality, inverse inequality, and (4.7) it holds

$$\begin{aligned} |c_h^{\text{R}}(\tilde{\mathbf{u}}, \boldsymbol{\eta}, \phi_h)| &\lesssim \|\mathbf{u}\|_{\mathbf{L}^\infty} \|\nabla_h \boldsymbol{\eta}^{\text{R}}\| \|\phi_h^{\text{R}}\| + \|\mathbf{u}\|_{\mathbf{L}^\infty} \sum_{F \in \mathcal{F}^0} h_F^{-\frac{1}{2}} \|[[\boldsymbol{\eta}^{\text{R}}]]\|_F h_F^{\frac{1}{2}} \|[[\phi_h^{\text{R}}]]\|_F \\ &\lesssim \|\mathbf{u}\|_{\mathbf{L}^\infty} (\|h_{\mathcal{T}}^{-1} \boldsymbol{\eta}^{\text{R}}\| + \|\nabla_h \boldsymbol{\eta}^{\text{R}}\|) \|\phi_h^{\text{R}}\| \lesssim \|\mathbf{u}\|_{\mathbf{L}^\infty} \|h_{\mathcal{T}}^{-1} \boldsymbol{\eta}^{\text{R}}\| \|\phi_h^{\text{R}}\|, \\ |c_h^{\text{R}}(\boldsymbol{\eta}, \Pi_h^{\text{St}} \mathbf{u}, \phi_h)| &\lesssim \|\nabla_h (\Pi_h^{\text{St}} \mathbf{u})^{\text{R}}\|_{\mathbf{L}^\infty} \|\boldsymbol{\eta}^s\| \|\phi_h^{\text{R}}\| \lesssim \|h_{\mathcal{T}}^{-1} (\Pi_h^{\text{St}} \mathbf{u})^{\text{R}}\|_{\mathbf{L}^\infty} \|\boldsymbol{\eta}^s\| \|\phi_h^{\text{R}}\| \\ &\lesssim \|\nabla \mathbf{u}\|_{\mathbf{L}^\infty} \|\boldsymbol{\eta}^s\| \|\phi_h^{\text{R}}\|, \end{aligned}$$

and

$$\begin{aligned} |c_h^{\text{R}}(\phi_h, \Pi_h^{\text{St}} \mathbf{u}, \phi_h)| &\lesssim \|\nabla_h (\Pi_h^{\text{St}} \mathbf{u})^{\text{R}}\|_{\mathbf{L}^\infty} \|\phi_h^s\| \|\phi_h^{\text{R}}\| + \|(\Pi_h^{\text{St}} \mathbf{u})^{\text{R}}\|_{\mathbf{L}^\infty} \sum_{F \in \mathcal{F}^0} \|\phi_h^s \cdot \mathbf{n}\|_F \|[[\phi_h^{\text{R}}]]\|_F \\ &\lesssim \|h_{\mathcal{T}}^{-1} (\Pi_h^{\text{St}} \mathbf{u})^{\text{R}}\|_{\mathbf{L}^\infty} \left(\|\phi_h^s\| \|\phi_h^{\text{R}}\| + \sum_{F \in \mathcal{F}^0} h_F \|\phi_h^s \cdot \mathbf{n}\|_F \|[[\phi_h^{\text{R}}]]\|_F \right) \\ &\lesssim \|\nabla \mathbf{u}\|_{\mathbf{L}^\infty} \|\phi_h^s\| \|\phi_h^{\text{R}}\|. \end{aligned}$$

Then (4.21) follows immediately. This completes the proof. \square

The terms produced by c_h^{R} in Lemma 4.21 can be stabilized by one of the two stabilizations \mathcal{S}_1 or \mathcal{S}_2 . For $\mathcal{S} = \mathcal{S}_1$, one can employ the Gronwall inequality. For $\mathcal{S} = \mathcal{S}_2$, techniques similar to the ones from the analysis of grad-div stabilizations [14] are applicable. In preparation for that, the following lemma states an intermediate estimate for the full convection term.

Lemma 4.8. *In view of the two stabilizations \mathcal{S}_1 and \mathcal{S}_2 , the following two estimates hold:*

$$|c_h^{\text{R}}(\mathbf{u}_h, \mathbf{u}_h, \phi_h)| \lesssim \begin{cases} \|\mathbf{u}\|_{\mathbf{L}^\infty} \|h_{\mathcal{T}}^{-1} \boldsymbol{\eta}^{\text{R}}\|^2 + \|\nabla \mathbf{u}\|_{\mathbf{L}^\infty} (\|\boldsymbol{\eta}^s\|^2 + \|\phi_h^s\|^2) + \|\mathbf{u}\|_{\mathbf{W}^{1, \infty}} \|\phi_h^{\text{R}}\|^2 & \text{for } \mathcal{S}_1, \\ \frac{1}{\gamma} \|\mathbf{u}\|_{\mathbf{L}^\infty}^2 \|h_{\mathcal{T}}^{-\frac{1}{2}} \boldsymbol{\eta}^{\text{R}}\|^2 + \frac{1}{\gamma} \|h_{\mathcal{T}}^{\frac{1}{2}} \nabla \mathbf{u}\|_{\mathbf{L}^\infty}^2 (\|\boldsymbol{\eta}^s\|^2 + \|\phi_h^s\|^2) + \frac{\gamma}{4} \|h_{\mathcal{T}}^{-\frac{1}{2}} \phi_h^{\text{R}}\|^2 & \text{for } \mathcal{S}_2. \end{cases}$$

According to (4.19), a combination with Lemma 4.6 immediately implies

$$(4.22) \quad \begin{aligned} |c_h^{\text{vol}}(\tilde{\mathbf{u}}, \tilde{\mathbf{u}}, \phi_h) - c_h^{\text{vol}}(\mathbf{u}_h, \mathbf{u}_h, \phi_h)| &\lesssim \|\mathbf{u}\|_{\mathbf{L}^\infty} \left(\|\nabla_h \boldsymbol{\eta}^{\text{S}}\|^2 + \|h_{\mathcal{T}}^{-1} \boldsymbol{\eta}^{\text{R}}\|^2 \right) \\ &+ (1 + h^{-2}) \|\nabla \mathbf{u}\|_{\mathbf{L}^\infty} \|\boldsymbol{\eta}^{\text{S}}\|^2 + \|\mathbf{u}\|_{\mathbf{W}^{1,\infty}} \left(\|\phi_h^{\text{S}}\|^2 + \|\phi_h^{\text{R}}\|^2 \right), \end{aligned}$$

and

$$(4.23) \quad \begin{aligned} |c_h^{\text{vol}}(\tilde{\mathbf{u}}, \tilde{\mathbf{u}}, \phi_h) - c_h^{\text{vol}}(\mathbf{u}_h, \mathbf{u}_h, \phi_h)| &\lesssim \|\mathbf{u}\|_{\mathbf{L}^\infty} \|\nabla_h \boldsymbol{\eta}^{\text{S}}\|^2 \\ &+ \frac{1}{\gamma} \|\mathbf{u}\|_{\mathbf{L}^\infty}^2 \|h_{\mathcal{T}}^{-\frac{1}{2}} \boldsymbol{\eta}^{\text{R}}\|^2 + \frac{1}{\gamma} \|h_{\mathcal{T}}^{\frac{1}{2}} \nabla \mathbf{u}\|_{\mathbf{L}^\infty}^2 \|\boldsymbol{\eta}^{\text{S}}\|^2 + (1 + h^{-2}) \|\nabla \mathbf{u}\|_{\mathbf{L}^\infty} \|\boldsymbol{\eta}^{\text{S}}\|^2 \\ &+ \left(\|\mathbf{u}\|_{\mathbf{W}^{1,\infty}} + \frac{1}{\gamma} \|h_{\mathcal{T}}^{\frac{1}{2}} \nabla \mathbf{u}\|_{\mathbf{L}^\infty}^2 \right) \|\phi_h^{\text{S}}\|^2 + \frac{\gamma}{4} \|h_{\mathcal{T}}^{-\frac{1}{2}} \phi_h^{\text{R}}\|^2. \end{aligned}$$

Proof. Estimates (4.22) and (4.23) follow from (4.21) and some differently weighted Young inequalities. The other estimates follow with Lemma 4.6 and a triangle inequality. \square

Theorem 4.9. *Let \mathbf{u} be the solution of (1.2) and \mathbf{u}_h be the solution of (3.5). Assume that $\mathbf{u} \in L^2((0, T]; \mathbf{W}^{1,\infty}(\Omega))$ and $\mathbf{u}_h^0 = \Pi_h^{\text{St}} \mathbf{u}(0)$. Under Assumption 4.1 it holds for $\mathcal{S} = \mathcal{S}_1$:*

$$(4.24) \quad \begin{aligned} E(e_h(T)) + \frac{\gamma}{2} \|e_h^{\text{R}}(T)\|^2 + \int_0^T \nu \|e_h\|^2 dt &\leq E(\boldsymbol{\eta}(T)) + \frac{\gamma}{2} \|\boldsymbol{\eta}^{\text{R}}(T)\|^2 \\ &+ \int_0^T \nu \|\boldsymbol{\eta}\|^2 dt + e^{K_1(\mathbf{u}, T)} \int_0^T \left\{ TE(\partial_t \boldsymbol{\eta}) + C\nu \|\boldsymbol{\eta}\|^2 + \frac{\gamma T}{2} \|\partial_t \boldsymbol{\eta}^{\text{R}}\|^2 \right. \\ &\left. + C\|\mathbf{u}\|_{\mathbf{L}^\infty} \left(\|\nabla_h \boldsymbol{\eta}^{\text{S}}\|^2 + \|h_{\mathcal{T}}^{-1} \boldsymbol{\eta}^{\text{R}}\|^2 \right) + C(1 + h^{-2}) \|\nabla \mathbf{u}\|_{\mathbf{L}^\infty} \|\boldsymbol{\eta}^{\text{S}}\|^2 \right\} dt, \end{aligned}$$

and for $\mathcal{S} = \mathcal{S}_2$:

$$(4.25) \quad \begin{aligned} E(e_h(T)) + \int_0^T \nu \|e_h\|^2 dt + \frac{\gamma}{2} \|h_{\mathcal{T}}^{-\frac{1}{2}} e_h^{\text{R}}\|^2 &\leq E(\boldsymbol{\eta}(T)) + \int_0^T \nu \|\boldsymbol{\eta}\|^2 dt \\ &+ \int_0^T \frac{\gamma}{2} \|h_{\mathcal{T}}^{-\frac{1}{2}} \boldsymbol{\eta}^{\text{R}}\|^2 dt + e^{K_2(\mathbf{u}, T)} \int_0^T \left\{ TE(\partial_t \boldsymbol{\eta}) + C\nu \|\boldsymbol{\eta}\|^2 + \frac{\gamma}{2} \|h_{\mathcal{T}}^{-\frac{1}{2}} \boldsymbol{\eta}^{\text{R}}\|^2 \right. \\ &+ C \left[\|\mathbf{u}\|_{\mathbf{L}^\infty} \|\nabla_h \boldsymbol{\eta}^{\text{S}}\|^2 + \frac{1}{\gamma} \|\mathbf{u}\|_{\mathbf{L}^\infty}^2 \|h_{\mathcal{T}}^{-\frac{1}{2}} \boldsymbol{\eta}^{\text{R}}\|^2 + \frac{1}{\gamma} \|h_{\mathcal{T}}^{\frac{1}{2}} \nabla \mathbf{u}\|_{\mathbf{L}^\infty}^2 \|\boldsymbol{\eta}^{\text{S}}\|^2 \right. \\ &\left. \left. + (1 + h^{-2}) \|\nabla \mathbf{u}\|_{\mathbf{L}^\infty} \|\boldsymbol{\eta}^{\text{S}}\|^2 \right] \right\} dt, \end{aligned}$$

where

$$\begin{aligned} K_1(\mathbf{u}, T) &:= 1 + \gamma/2 + C(1 + \frac{1}{\gamma}) \|\mathbf{u}\|_{L^1((0, T]; \mathbf{W}^{1,\infty}(\Omega))}, \\ K_2(\mathbf{u}, T) &:= 1 + C \left(\|\mathbf{u}\|_{L^1((0, T]; \mathbf{W}^{1,\infty}(\Omega))} + \frac{1}{\gamma} \|h_{\mathcal{T}}^{\frac{1}{2}} \nabla \mathbf{u}\|_{L^2((0, T]; \mathbf{L}^\infty(\Omega))} \right). \end{aligned}$$

Proof. Direct calculations imply

$$(4.26) \quad \mathcal{S}_1(\phi_h, \phi_h) = \frac{1}{2} \frac{d}{dt} \|\phi_h^{\text{R}}\|^2, \quad |\mathcal{S}_1(\boldsymbol{\eta}, \phi_h)| \leq \frac{T}{2} \|\partial_t \boldsymbol{\eta}^{\text{R}}\|^2 + \frac{1}{2T} \|\phi_h^{\text{R}}\|^2,$$

$$(4.27) \quad \mathcal{S}_2(\phi_h, \phi_h) = \|h_{\mathcal{T}}^{-\frac{1}{2}} \phi_h^{\text{R}}\|^2, \quad |\mathcal{S}_2(\boldsymbol{\eta}, \phi_h)| \leq \frac{1}{2} \|h_{\mathcal{T}}^{-\frac{1}{2}} \boldsymbol{\eta}^{\text{R}}\|^2 + \frac{1}{2} \|h_{\mathcal{T}}^{-\frac{1}{2}} \phi_h^{\text{R}}\|^2.$$

For $i = 1$ (i.e., $\mathcal{S} = \mathcal{S}_1$), a combination of (4.18), (4.15), (4.16), (4.26), and (4.22) gives

$$\begin{aligned} \frac{d}{dt}E(\phi_h) + \frac{\gamma}{2}\frac{d}{dt}\|\phi_h^R\|^2 + \frac{\nu}{2}\|\phi_h\|^2 &\leq TE(\partial_t\boldsymbol{\eta}) + \frac{1}{T}E(\phi_h) + C\nu\|\boldsymbol{\eta}\|^2 \\ &\quad + \frac{\gamma T}{2}\|\partial_t\boldsymbol{\eta}^R\|^2 + \frac{\gamma}{2T}\|\phi_h^R\|^2 + C\|\mathbf{u}\|_{\mathbf{L}^\infty} \left(\|\nabla_h\boldsymbol{\eta}^s\|^2 + \|h_{\mathcal{T}}^{-1}\boldsymbol{\eta}^R\|^2 \right) \\ &\quad + C(1+h^{-2})\|\nabla\mathbf{u}\|_{\mathbf{L}^\infty}\|\boldsymbol{\eta}^s\|^2 + C\|\mathbf{u}\|_{\mathbf{W}^{1,\infty}} \left(\|\phi_h^s\|^2 + \|\phi_h^R\|^2 \right). \end{aligned}$$

Since $\|\phi_h^s\|^2 \leq 2E(\phi_h)$ and $\|\phi_h^R\|^2 = \frac{2}{\gamma} * \frac{\gamma}{2}\|\phi_h^R\|^2$, the Gronwall lemma yields

$$\begin{aligned} E(\phi_h(T)) + \frac{\gamma}{2}\|\phi_h^R(T)\|^2 + \int_0^T \frac{\nu}{2}\|\phi_h\|^2 dt \\ \leq e^{K_1(\mathbf{u},T)} \int_0^T \left\{ TE(\partial_t\boldsymbol{\eta}) + C\nu\|\boldsymbol{\eta}\|^2 + \frac{\gamma T}{2}\|\partial_t\boldsymbol{\eta}^R\|^2 \right. \\ \left. + C\|\mathbf{u}\|_{\mathbf{L}^\infty} \left(\|\nabla_h\boldsymbol{\eta}^s\|^2 + \|h_{\mathcal{T}}^{-1}\boldsymbol{\eta}^R\|^2 \right) + C(1+h^{-2})\|\nabla\mathbf{u}\|_{\mathbf{L}^\infty}\|\boldsymbol{\eta}^s\|^2 \right\} dt. \end{aligned}$$

Then (4.24) follows. For $i = 2$ (i.e., $\mathcal{S} = \mathcal{S}_2$), a combination of (4.18), (4.15), (4.16), (4.27), and (4.23) leads to

$$\begin{aligned} \frac{d}{dt}E(\phi_h) + \frac{\nu}{2}\|\phi_h\|^2 + \frac{\gamma}{4}\|h_{\mathcal{T}}^{-\frac{1}{2}}\phi_h^R\|^2 &\leq TE(\partial_t\boldsymbol{\eta}) + \frac{1}{T}E(\phi_h) + C\nu\|\boldsymbol{\eta}\|^2 \\ &\quad + \frac{\gamma}{2}\|h_{\mathcal{T}}^{-\frac{1}{2}}\boldsymbol{\eta}^R\|^2 + C \left[\|\mathbf{u}\|_{\mathbf{L}^\infty}\|\nabla_h\boldsymbol{\eta}^s\|^2 + \frac{1}{\gamma}\|\mathbf{u}\|_{\mathbf{L}^\infty}^2\|h_{\mathcal{T}}^{-\frac{1}{2}}\boldsymbol{\eta}^R\|^2 + \frac{1}{\gamma}\|h_{\mathcal{T}}^{\frac{1}{2}}\nabla\mathbf{u}\|_{\mathbf{L}^\infty}^2\|\boldsymbol{\eta}^s\|^2 \right. \\ &\quad \left. + (1+h^{-2})\|\nabla\mathbf{u}\|_{\mathbf{L}^\infty}\|\boldsymbol{\eta}^s\|^2 + \left(\|\mathbf{u}\|_{\mathbf{W}^{1,\infty}} + \frac{1}{\gamma}\|h_{\mathcal{T}}^{\frac{1}{2}}\nabla\mathbf{u}\|_{\mathbf{L}^\infty}^2 \right) \|\phi_h^s\|^2 \right]. \end{aligned}$$

Also by Gronwall lemma we have

$$\begin{aligned} E(\phi_h(T)) + \int_0^T \frac{\nu}{2}\|\phi_h\|^2 + \frac{\gamma}{4}\|h_{\mathcal{T}}^{-\frac{1}{2}}\phi_h^R\|^2 dt \\ \leq e^{K_2(\mathbf{u},T)} \int_0^T \left\{ TE(\partial_t\boldsymbol{\eta}) + C\nu\|\boldsymbol{\eta}\|^2 + \frac{\gamma}{2}\|h_{\mathcal{T}}^{-\frac{1}{2}}\boldsymbol{\eta}^R\|^2 \right. \\ \left. + C \left[\|\mathbf{u}\|_{\mathbf{L}^\infty}\|\nabla_h\boldsymbol{\eta}^s\|^2 + \frac{1}{\gamma}\|\mathbf{u}\|_{\mathbf{L}^\infty}^2\|h_{\mathcal{T}}^{-\frac{1}{2}}\boldsymbol{\eta}^R\|^2 + \frac{1}{\gamma}\|h_{\mathcal{T}}^{\frac{1}{2}}\nabla\mathbf{u}\|_{\mathbf{L}^\infty}^2\|\boldsymbol{\eta}^s\|^2 \right. \right. \\ \left. \left. + (1+h^{-2})\|\nabla\mathbf{u}\|_{\mathbf{L}^\infty}\|\boldsymbol{\eta}^s\|^2 \right] \right\} dt. \end{aligned}$$

Then (4.25) follows. This completes the proof. \square

5. THE REDUCED SCHEME

This section discusses a possible condensation of all enrichment and all higher order pressure degrees of freedom. Here we proceed similarly to the Stokes case explained in [25].

In order to remove all higher order pressure degrees of freedom a larger enrichment space \mathbf{V}_h^R has to be used, i.e.,

$$\mathbf{V}_h^R := \begin{cases} \widetilde{\mathbf{RT}}_{k-1}^{\text{int}}(\mathcal{T}) & k \geq d, \\ (\mathbf{RT}_0(\mathcal{T}) \cap \mathbf{H}_0(\text{div}, \Omega)) \oplus \widetilde{\mathbf{RT}}_{k-1}^{\text{int}}(\mathcal{T}) & k < d. \end{cases}$$

The condensation of \mathbf{RT}_0 DoFs and higher order Raviart–Thomas bubbles are based on different principles. For the \mathbf{RT}_0 DoFs, from [32, Lemma 3.2] it is not hard to see that the mass lumping for the $\mathbf{RT}_0 - \mathbf{RT}_0$ block from the time and diffusion discretizations does not affect the accuracy. Then the static condensation of \mathbf{RT}_0 unknowns is possible in case that the discretization of the nonlinear term does not contribute to the $\mathbf{RT}_0 - \mathbf{RT}_0$ block, e.g., $c_h(\cdot, \cdot, \cdot)$ is linearized with a Picard iteration. For higher order Raviart–Thomas bubbles, based on the fact that the divergence operator on the chosen higher order enrichment space is injective, this part of the velocity solution is indeed uniquely determined by the divergence of the \mathbf{H}^1 part due to the divergence constraint. Therefore for each \mathbf{H}^1 shape function there is a unique attached Raviart–Thomas function to eliminate the higher order part of its divergence. Seeking the solution in a subspace spanned by these Raviart–Thomas attached \mathbf{H}^1 basis functions leads to a reduced $\mathbf{P}_k - P_0$ scheme, where the higher order pressure DoFs are no longer needed as Lagrange multipliers. In conclusion, the condensation of \mathbf{RT}_0 unknowns is due to the diagonal matrix structure of the $\mathbf{RT}_0 - \mathbf{RT}_0$ block, while the condensation of the higher order Raviart–Thomas bubbles, as well as higher order pressure DoFs, is due to the incompressibility constraint, which is always available as long as the model is incompressible. Also note, that the sparsity pattern of the resulting system is the same as that of a classical $\mathbf{P}_k \times P_0$ method for $k \geq d$, because the interior \mathbf{RT} bubbles on one cell do not couple with the all degrees of freedom of any other cell in the original method.

In what follows the implementation of the reduced scheme on the algebraic level is shortly discussed. For simplicity we use the case $k \geq d$ and the case where the nonlinear term is treated explicitly as an example.

To handle the nonlinear term, one possibility is to put it explicitly on the right-hand side, such that the matrix stays constant throughout the whole simulation (if the time step is constant). Then, algebraically the full linear system in each nonlinear iteration within a time step has the form

$$\begin{pmatrix} D_{cc} + A_{cc} & (D_{Rc} + A_{Rc})^\top & B_c^\top \\ D_{Rc} - A_{Rc} & D_{RR} + A_{RR} + S_{RR} & B_R^\top \\ B_c & B_R & 0 \end{pmatrix} \begin{pmatrix} U_c \\ U_R \\ P \end{pmatrix} = \begin{pmatrix} F_c \\ F_R \\ 0 \end{pmatrix}.$$

Here, the A -blocks refer to the linear Stokes operators, the D -blocks refer to the mass matrix and F contains all right-hand side terms from f , the nonlinear term and the previous time step. The matrix S_{RR} refers to the used stabilization S_1 or S_2 for the enrichment part.

Following [25] we employ a reconstruction operator $\mathcal{R} : \mathbf{V}_h^{\text{ct}} \rightarrow \mathbf{V}_h^{\text{R}}$ and its representation matrix R . Recall, that the enrichment part is uniquely determined by $U_R = -RU_c$. With that, the problem can be reduced to solving

$$\begin{pmatrix} D_{cc} + A_{cc} + (D_{Rc} - A_{Rc})^\top R + R^\top (D_{Rc} + A_{Rc}) & B_{0,c}^\top \\ B_{0,c} & 0 \end{pmatrix} \begin{pmatrix} U_c \\ P_0 \end{pmatrix} = \begin{pmatrix} F_c - R^\top F_R \\ 0 \end{pmatrix}.$$

Here, P_0 refers to the piecewise constant pressure and $B_{0,\text{ct}}$ to the div-pressure matrix between velocities of \mathbf{V}_h^{c} and P_0 pressures. Also the full pressure can be recovered by solving small local problems. All details can be found in [25] as there are no additional difficulties if the nonlinear term is handled explicitly in the right-hand side.

6. NUMERICAL EXAMPLES

This section demonstrates the performance of the proposed schemes in two benchmark examples. Concerning the nonlinear solver a Picard iteration scheme was employed and

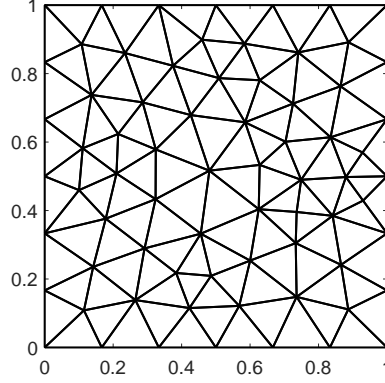


FIGURE 6.1. Initial grid for Example 1.

terminated when the difference to the last iteration in the H^1 -norm is below the tolerance 10^{-8} . The enrichment spaces \mathbf{V}_h^R are built from the basis functions constructed in [25].

6.1. **Example 1.** The first example from [16, Example 4.2] takes the inhomogeneous data such that it matches the flow

$$\begin{aligned} \mathbf{u}(x, y, t) &= 2\pi \sin(\pi t) \begin{pmatrix} \sin(\pi x)^2 \sin(\pi y) \cos(\pi y) \\ -\sin(\pi y)^2 \sin(\pi x) \cos(\pi x) \end{pmatrix}, \\ p(x, y, t) &= 20 \sin(\pi t)(x^2 y - 1/6) \end{aligned}$$

for $\nu = 10^{-6}$ and computes the discrete \mathbf{u}_h and p_h with the Crank–Nicolson scheme with time step $\tau = 10^{-4}$ until $T = 3$ unstructured meshes, the initial mesh is depicted in Figure 6.1. The parameter of \mathcal{S} , γ , is taken as 1 always. Figures 6.2–6.4 display results for orders $k \in \{2, 3, 4\}$ for the maximal L^2 error in time and the full estimated norm in Theorems 4.5 and 4.9, i.e.,

$$|||\mathbf{u}|||_*^2 := \|\mathbf{u}^s\|^2 + \nu \int_0^T \|\nabla \mathbf{u}^{\text{ct}}\|^2 dt + \begin{cases} \|\mathbf{u}^R\|^2 & \text{for (3.3) with } \mathcal{S}_1, \\ \int_0^T \|h_T^{\frac{1}{2}} \nabla \cdot \mathbf{u}^R\|^2 dt & \text{for (3.3) with } \mathcal{S}_2, \\ \int_0^T |\mathbf{u}|_{\mathbf{u}_h, \text{uw}}^2 dt & \text{for upwind DG.} \end{cases}$$

It can be seen that all stabilizations attain at least their estimated convergence orders and that the upwind stabilization yields the best results among the three tested stabilizations. The upwind stabilization even shows a better convergence rate pre-asymptotically. The easier to implement stabilization \mathcal{S}_2 yields the second-best results. Surprisingly, the asymptotic convergence rates for $k = 3$ are much better than expected from the theory.

Figure 6.5 provides some study on convection-robustness and depicts the maximal L^2 error for the reduced schemes of order $k \in \{2, 3, 4\}$ with stabilization \mathcal{S}_2 and a second-order classical Taylor–Hood method with skew-symmetric discretization of the nonlinear convection term for different choices of $\nu \in \{10^{-2}, 10^{-4}, 10^{-6}\}$. Here, two observations are in order. First, the Raviart–Thomas enriched methods are convection-robust for all three stabilizations in the sense that the errors are relatively insensitive to ν . Second, the Taylor–Hood method shows a large increase in the error when going from $\nu = 10^{-2}$ to $\nu = 10^{-4}$ which indicates that this method is not convection-robust. Note however, that the Taylor–Hood method can be improved by adding grad-div stabilization to have similar results and was just added in this form to show the behavior of a non-convection-robust scheme.

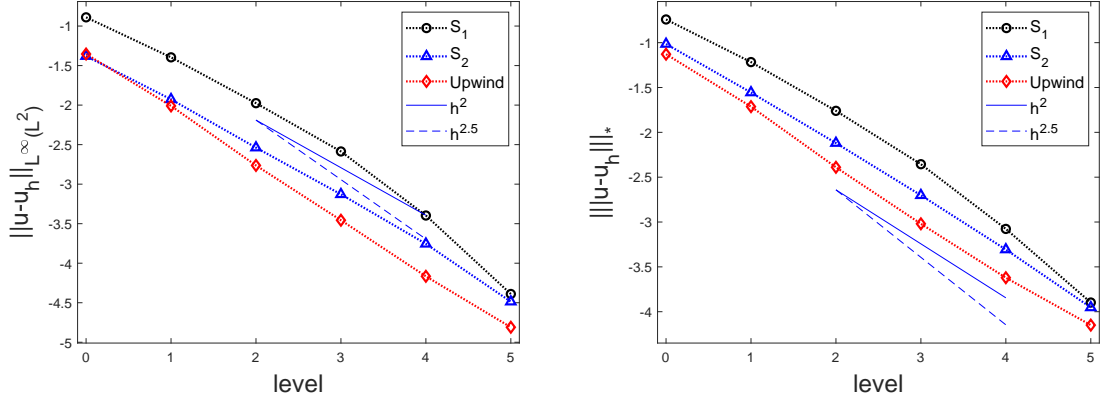


FIGURE 6.2. Example 1: Convergence rates of $\|\mathbf{u} - \mathbf{u}_h^S\|_{L^\infty(L^2)}$ (energy error, left) and $\|(\mathbf{u}, 0) - \mathbf{u}_h\|_*$ (right) from the estimate with $\nu = 10^{-6}$, $\Delta t = 10^{-4}$, and $T = 3$ for the reduced $P_2 - P_0$ scheme.

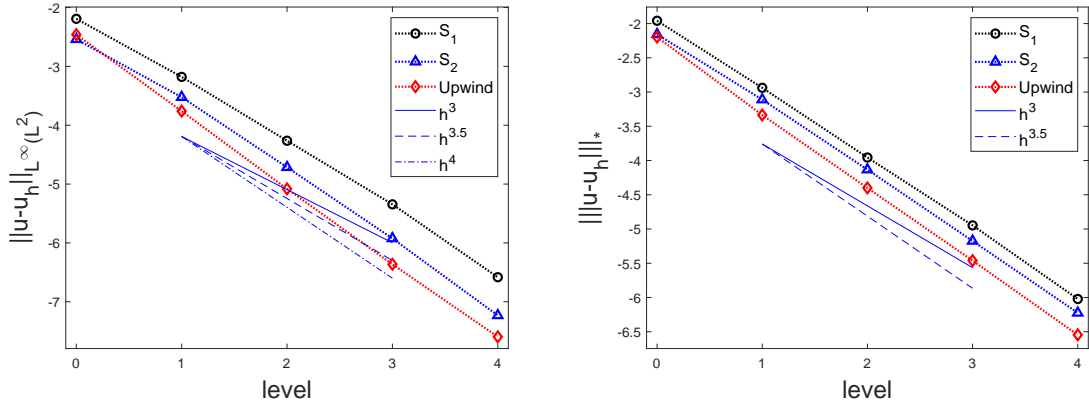


FIGURE 6.3. Example 1: Convergence rates of $\|\mathbf{u} - \mathbf{u}_h^S\|_{L^\infty(L^2)}$ (energy error, left) and $\|(\mathbf{u}, 0) - \mathbf{u}_h\|_*$ (right) from the estimate with $\nu = 10^{-6}$, $\Delta t = 10^{-4}$, and $T = 3$ for the reduced $P_3 - P_0$ scheme.

Finally, Table 6.1 compares the numerical costs for the full and reduced scheme with S_2 stabilization and a Taylor–Hood scheme with skew-symmetric convection term (SKEW) and grad-div stabilization of the same order for $k \in \{2, 3, 4\}$. This time, the grad-div stabilization was added such that all methods do exactly two implicit Picard iterations in each time step (so altogether 10.000 Picard iterations for 5.000 time steps). The direct sparse matrix solver Pardiso [43] is used. For the first iteration in each of the first 7 time steps, a complete solver (symbolic factorization + numerical factorization + forward and backward substitutions) is employed. The simulation was done on a laptop with an 11th Gen Intel(R) Core(TM) i5-11400H CPU with 6 cores. For all other iterations we keep the symbolic factorization of the sparse matrix. The table reports the number of degrees of freedom, nonzeros in the system matrix and solver times in each case. It can be seen, that the reduction procedure significantly reduces the numerical costs and that the full scheme, despite the larger number

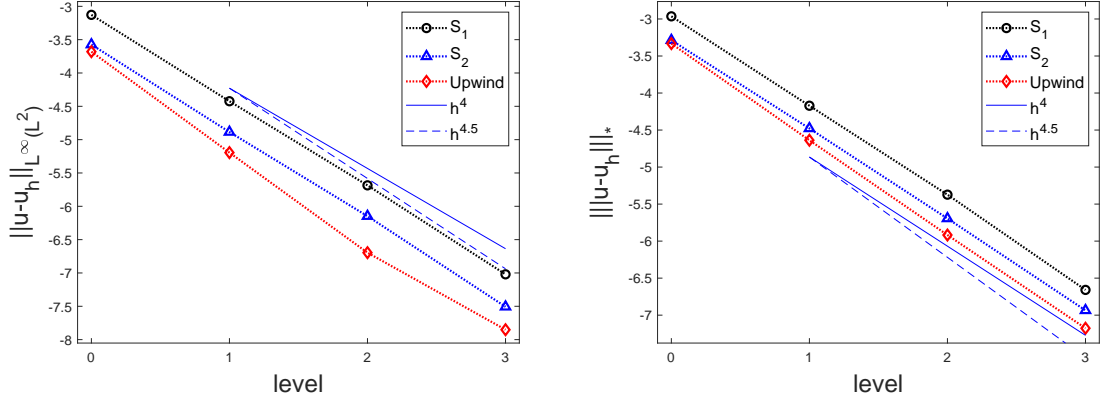


FIGURE 6.4. Example 1: Convergence rates of $\|u - u_h^s\|_{L^\infty(L^2)}$ (energy error, left) and $\|(u, 0) - u_h\|_*$ (right) from the estimate with $\nu = 10^{-6}$, $\Delta t = 10^{-4}$, and $T = 3$ for the reduced $P_4 - P_0$ scheme.

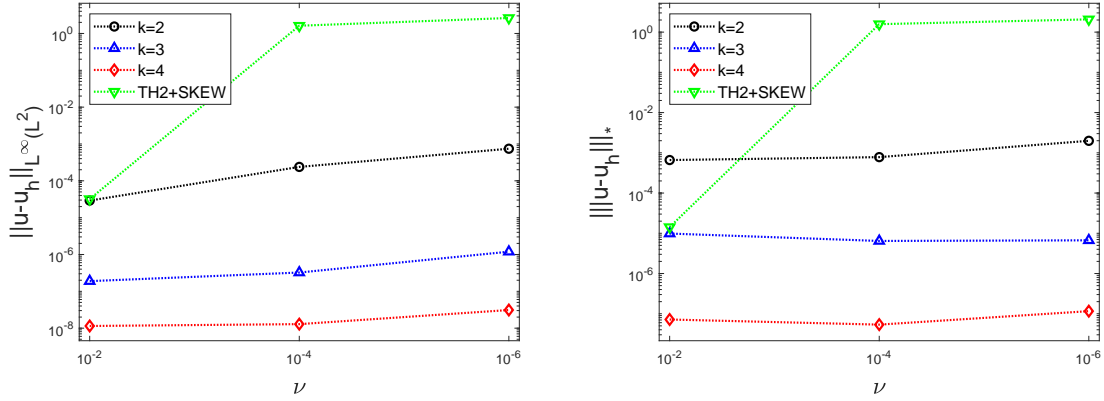


FIGURE 6.5. Example 1: Plots of $\|u - u_h^s\|_{L^\infty(L^2)}$ (energy error, left) and $\|(u, 0) - u_h\|_*$ (right) from the estimate over $\nu \in \{10^{-2}, 10^{-4}, 10^{-6}\}$ with $\Delta t = 10^{-4}$ and $T = 3$ for the reduced and S_2 stabilized $P_k - P_0$ schemes ($k \in \{2, 3, 4\}$) on mesh level 3.

of degrees of freedom, has comparable numerical costs and solver times to a Taylor–Hood scheme.

6.2. Example 2. This example considers the Kelvin–Helmholtz instability benchmark problem for which reference values are computed and discussed in [44]. Here, the case of Reynolds number $Re = 10.000$ and the initial condition

$$\mathbf{u}^0(x, y) = \begin{pmatrix} u_\infty \tanh\left(\frac{2y-1}{\delta_0}\right) \\ 0 \end{pmatrix} + c_n \begin{pmatrix} -\partial_y \psi(x, y) \\ \partial_x \psi(x, y) \end{pmatrix}$$

with the stream function

$$\psi(x, y) = u_\infty \exp\left(-\frac{(y-0.5)^2}{\delta_0^2}\right) (\cos(8\pi x) + \cos(20\pi x))$$

TABLE 6.1. Example 1: Number of DoFs, number of nonzero entries of the coefficient matrix A , and cost of the proposed method (with \mathcal{S}_2 stabilization) and Taylor–Hood element method (with SKEW and grad-div stabilization scaled by h) on mesh level 3 (7424 elements), with $\Delta t = 10^{-4}$ and $T = 0.5$ (which amounts to totally 5000 time steps and 10000 Picard iterations in every method). Cost_1 : total computing time in seconds. Cost_2 : total computing time in seconds on Pardiso. Cost_3 : mean computing time in seconds per iteration where a complete solver is used.

Order	Method	$\#\{\mathbf{u}$ DoFs}	$\#\{p$ DoFs}	$\#\{\text{nz}(A)\}$	Cost_1	Cost_2	Cost_3
$k = 2$	Full	44930	22272	1718 K	2.31e3	1.23e3	0.5804
	Reduced	30082	7424	872 K	1.78e3	8.44e2	0.3777
	TH	30082	3809	974 K	1.85e3	1.07e3	0.4213
$k = 3$	Full	89666	44544	5329 K	5.50e3	2.81e3	1.4144
	Reduced	67394	7424	2582 K	4.22e3	2.06e3	0.7799
	TH	67394	15041	3559 K	5.86e3	3.81e3	1.2671
$k = 4$	Full	149250	74240	12615 K	1.12e4	5.57e3	2.8217
	Reduced	119554	7424	6045 K	8.20e3	3.80e3	1.5864
	TH	119554	33697	9211 K	1.39e4	9.17e3	2.9569

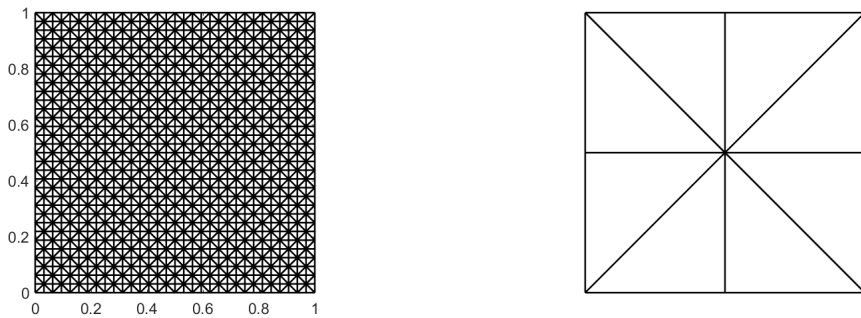


FIGURE 6.6. Example 2: A mesh consisting of 32×32 divided squares (left) built by repeating a 2×2 squared structure (right).

is studied, where the parameters are chosen to be $\delta_0 = 1/28$, $u_\infty = 1$ and $c_n = 10^{-3}$. Via the relation $Re = \delta_0 u_\infty / \mu$, the viscosity is $\mu = 1/(Re\delta_0) = 1/280.000 \approx 3.57 \cdot 10^{-6}$. At the left and right boundary, i.e., for $x = 0$ and $x = 1$, periodic conditions are applied, while at the top and bottom boundary, i.e., for $y = 0$ and $y = 1$, free-slip conditions are applied.

This problem describes the successive pairing of vortices until finally only one rotating vortex remains. It is clearly convection-dominated so that a stabilized method, e.g., a convection-robust method, is necessary for performing stable numerical simulations. In [44] simulations were performed on grids up to 256×256 mesh cells and with a velocity space of polynomial degree 8. It was found that predicting a reference solution is quite challenging for the Reynolds number used in our simulations. In fact, a reference solution could be obtained only up to $t/\delta_0 = 200$, i.e., $t = 50/7 \approx 7.14$, which corresponds to the situation of two rotating vortices. It has been observed in [44] that the formation time of the final vortex and also its position is very sensitive to the setup and even tiny differences in algorithms (or even compiler options) can lead to a different behavior.

The example is simulated on structured and symmetric meshes like the one depicted in Figure 6.6 and for the polynomial order $k = 2$. For the time discretization, we employ the

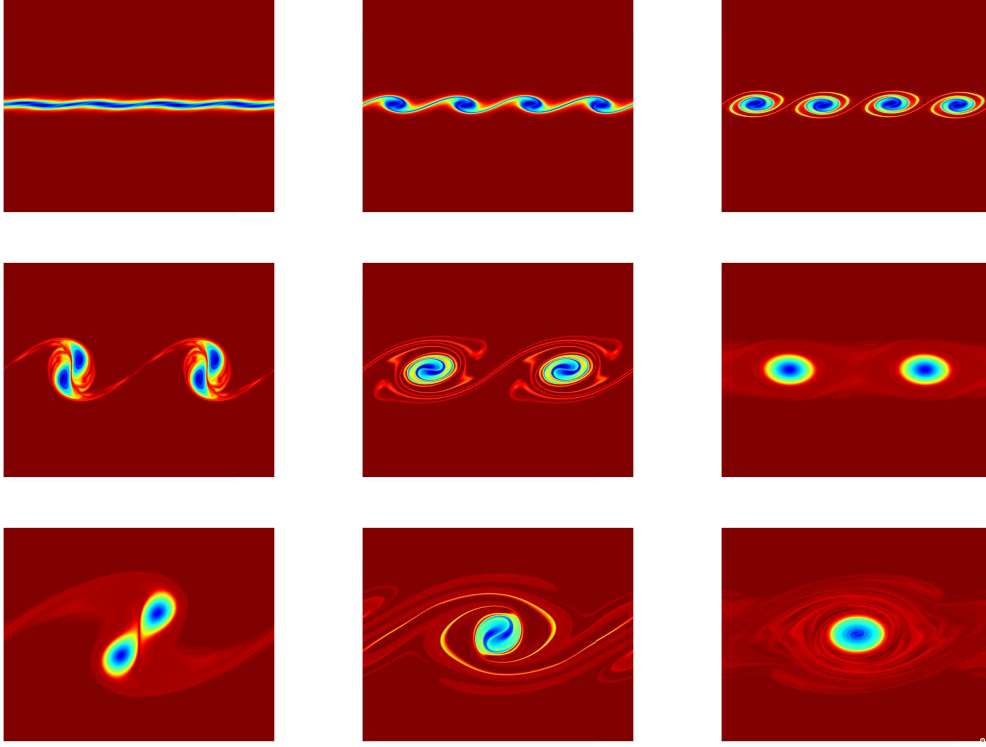


FIGURE 6.7. Example 2: From left to right and top to bottom, vorticity at $\bar{t} = 5, 10, 17, 34, 56, 200, 272, 308, 400$ on the mesh with 131072 cells.

Crank–Nicolson scheme with time step $\tau = 10^{-3}\delta_0$. Quantities of interest, besides the kinetic energy, comprise the enstrophy given by

$$\mathcal{E}(t, \mathbf{u}) := \frac{1}{2} \|\text{Curl}(\mathbf{u})\|_{L^2(\Omega)} \quad \text{with} \quad \text{Curl}(\mathbf{u}) := \partial_x u_2 - \partial_y u_1,$$

which should be monotonously decreasing in time, and the vorticity thickness defined by

$$\delta(t, \mathbf{u}) := \frac{2u_\infty}{\sup_{y \in [0,1]} \left| \int_0^1 \text{Curl}(\mathbf{u}) \, dx \right|},$$

where we approximate the supremum in the denominator by taking the maximum over all $y \in \{(1 + 2k)/2048 : k = 1, \dots, 1024\}$. In this example we try scheme (3.3) with stabilization \mathcal{S}_2 only and the parameter γ is chosen as 1 again.

The merging process of the vortices obtained from our method is shown in Figure 6.7. Figure 6.8 shows the evolution of these quantities in the performed simulation. Although our simulations were performed on relatively coarse meshes and low polynomial order of the velocity, we observe that the general qualitative behavior of the vorticity thickness and the enstrophy is inline with the expectations. The vorticity thickness shows the right kinks when the vortices are forming. Even for $t/\delta_0 > 200$, where no reference solution is available, the qualitative behavior of the results of the proposed scheme corresponds with those from [44].

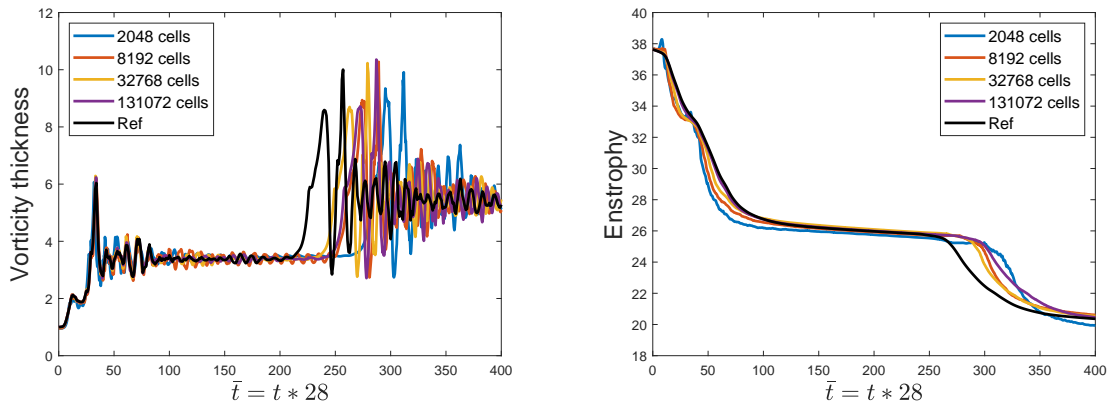


FIGURE 6.8. Example 2: Vorticity thickness (left) and enstrophy (right).

7. CONCLUSIONS AND OUTLOOK

This paper successfully extends the Raviart–Thomas enriched Scott–Vogelius elements from the stationary Stokes model problem [32, 25] to the full instationary Navier–Stokes problem. This results in a family of pressure-robust, divergence-free, EMA-preserving, and convection-robust methods. However, a stabilization for the Raviart–Thomas enrichment part is required. Three choices are analyzed, among them a grad-div like stabilization for the enrichment part and the upwind stabilization known from DG framework, and all of them can be used and ensure convergence of at least order k in the L^2 -norm at any time. One important advantage of the novel family is the possibility to reduce the scheme to a $P_k \times P_0$ scheme, which greatly reduces the number of unknowns and the computational costs without compromising any features listed above. All theoretical results are supported by numerical experiments, in particular by a simulation of the challenging two-dimensional Kelvin–Helmholtz benchmark problem.

Out of the scope of this paper but interesting aspects for future research are the application of the new family to real turbulent flows in three dimensions, the investigation of preconditioners and iterative solvers and additional convection stabilization, e.g., in the spirit of [2], to improve the order of convergence in convection-dominated regimes.

ACKNOWLEDGMENTS

Naveed Ahmed would like to acknowledge financial support from the Gulf University for Science and Technology for an internal Seed Grant (No. 278877). Xu Li was supported by the China Scholarship Council (No. 202106220106) and the National Natural Science Foundation of China (No. 12131014). Christian Merdon gratefully acknowledges the funding by the German Science Foundation (DFG) within the project “ME 4819/2-1”.

REFERENCES

- [1] R. Abramov and A. Majda. Discrete approximations with additional conserved quantities: deterministic and statistical behavior. *Methods Appl. Anal.*, 10(2):151–190, 2003.
- [2] N. Ahmed, G. R. Barrenechea, E. Burman, J. Guzmán, A. Linke, and C. Merdon. A pressure-robust discretization of Oseen’s equation using stabilization in the vorticity equation. *SIAM J. Numer. Anal.*, 59(5):2746–2774, 2021.
- [3] N. Ahmed, A. Linke, and C. Merdon. On really locking-free mixed finite element methods for the transient incompressible Stokes equations. *SIAM J. Numer. Anal.*, 56(1):185–209, 2018.

- [4] A. Allendes, G. R. Barrenechea, and J. Novo. A divergence-free stabilized finite element method for the evolutionary Navier–Stokes equations. *SIAM J. Sci. Comput.*, 43(6):A3809–A3836, 2021.
- [5] V. Anaya, A. Bouharguane, D. Mora, C. Reales, R. Ruiz-Baier, N. Seloula, and H. Torres. Analysis and approximation of a vorticity-velocity-pressure formulation for the Oseen equations. *J. Sci. Comput.*, 80(3):1577–1606, 2019.
- [6] D. Boffi, F. Brezzi, and M. Fortin. *Mixed finite element methods and applications*, volume 44 of *Springer Series in Computational Mathematics*. Springer, Heidelberg, 2013.
- [7] S. C. Brenner and L. R. Scott. *The mathematical theory of finite element methods*, volume 15 of *Texts in Applied Mathematics*. Springer, New York, third edition, 2008.
- [8] M. A. Case, V. J. Ervin, A. Linke, and L. G. Rebholz. A connection between Scott-Vogelius and grad-div stabilized Taylor-Hood FE approximations of the Navier-Stokes equations. *SIAM J. Numer. Anal.*, 49(4):1461–1481, 2011.
- [9] S. Charnyi, T. Heister, M. A. Olshanskii, and L. G. Rebholz. On conservation laws of Navier-Stokes Galerkin discretizations. *J. Comput. Phys.*, 337:289–308, 2017.
- [10] S. Charnyi, T. Heister, M. A. Olshanskii, and L. G. Rebholz. Efficient discretizations for the EMAC formulation of the incompressible Navier–Stokes equations. *Appl. Numer. Math.*, 141:220–233, 2019.
- [11] X. Chen, Y. Li, C. Drapaca, and J. Cimbala. Some continuous and discontinuous galerkin methods and structure preservation for incompressible flows. *Int. J. Numer. Meth. Fluids*, 93(7):2155–2174, 2021.
- [12] S. H. Christiansen and K. Hu. Generalized finite element systems for smooth differential forms and Stokes’ problem. *Numer. Math.*, 140(2):327–371, 2018.
- [13] B. Cockburn, G. Kanschat, and D. Schötzau. A note on discontinuous Galerkin divergence-free solutions of the Navier–Stokes equations. *J. Sci. Comput.*, 31(1-2):61–73, 2007.
- [14] J. de Frutos, B. Garcá Archilla, V. John, and J. Novo. Analysis of the grad-div stabilization for the time-dependent Navier–Stokes equations with inf-sup stable finite elements. *Adv. Comput. Math.*, 44(1):195–225, 2018.
- [15] J. A. Evans and T. J. R. Hughes. Isogeometric divergence-conforming B-splines for the unsteady Navier-Stokes equations. *J. Comput. Phys.*, 241:141–167, 2013.
- [16] B. García-Archilla, V. John, and J. Novo. On the convergence order of the finite element error in the kinetic energy for high Reynolds number incompressible flows. *Comput. Methods Appl. Mech. Engrg.*, 385:Paper No. 114032, 54, 2021.
- [17] V. Girault, R. H. Nochetto, and L. R. Scott. Max-norm estimates for Stokes and Navier-Stokes approximations in convex polyhedra. *Numer. Math.*, 131(4):771–822, 2015.
- [18] V. Girault and P.-A. Raviart. *Finite element methods for Navier–Stokes equations*, volume 5 of *Springer Series in Computational Mathematics*. Springer-Verlag, Berlin, 1986. Theory and algorithms.
- [19] J. Guzmán and M. Neilan. Conforming and divergence-free Stokes elements on general triangular meshes. *Math. Comp.*, 83(285):15–36, 2014.
- [20] J. Guzmán and M. Neilan. inf-sup stable finite elements on barycentric refinements producing divergence-free approximations in arbitrary dimensions. *SIAM J. Numer. Anal.*, 56(5):2826–2844, 2018.
- [21] J. Guzmán and L. R. Scott. Cubic Lagrange elements satisfying exact incompressibility. *SMAI J. Comput. Math.*, 4:345–374, 2018.
- [22] J. Guzmán, C.-W. Shu, and F. A. Sequeira. H(div) conforming and DG methods for incompressible Euler’s equations. *IMA J. Numer. Anal.*, 37(4):1733–1771, 2017.
- [23] Y. Han and Y. Hou. Robust error analysis of H(div)-conforming DG method for the time-dependent incompressible Navier–Stokes equations. *J. Comput. Appl. Math.*, 390:Paper No. 113365, 13, 2021.
- [24] V. John. *Finite element methods for incompressible flow problems*, volume 51 of *Springer Series in Computational Mathematics*. Springer, Cham, 2016.
- [25] V. John, X. Li, C. Merdon, and H. Rui. Inf-sup stabilized Scott–Vogelius pairs on general simplicial grids by Raviart–Thomas enrichment. *arXiv*, arXiv: 2206.01242, 2022.
- [26] V. John, A. Linke, C. Merdon, M. Neilan, and L. G. Rebholz. On the divergence constraint in mixed finite element methods for incompressible flows. *SIAM Rev.*, 59(3):492–544, 2017.
- [27] P. L. Lederer, C. Lehrenfeld, and J. Schöberl. Hybrid discontinuous Galerkin methods with relaxed H(div)-conformity for incompressible flows. Part I. *SIAM J Numer. Anal.*, 56(4):2070–2094, 2018.
- [28] P. L. Lederer, A. Linke, C. Merdon, and J. Schöberl. Divergence-free reconstruction operators for pressure-robust Stokes discretizations with continuous pressure finite elements. *SIAM J. Numer. Anal.*, 55(3):1291–1314, 2017.
- [29] C. Lehrenfeld. Hybrid discontinuous Galerkin methods for incompressible flow problems. Master’s thesis, RWTH Aachen, May 2010.

- [30] C. Lehrenfeld and J. Schöberl. High order exactly divergence-free hybrid discontinuous Galerkin methods for unsteady incompressible flows. *Comput. Methods Appl. Mech. Engrg.*, 307:339–361, 2016.
- [31] X. Li and H. Rui. An EMA-conserving, pressure-robust and Re-semi-robust reconstruction method for the unsteady incompressible Navier–Stokes equations. *arXiv*, arXiv:2108.08355, 2021. to be appeared in *ESAIM: Math. Model. Numer. Anal.*
- [32] X. Li and H. Rui. A low-order divergence-free H(div)-conforming finite element method for Stokes flows. *IMA J. Numer. Anal.*, 2021. Published online.
- [33] A. Linke. On the role of the Helmholtz decomposition in mixed methods for incompressible flows and a new variational crime. *Comput. Methods Appl. Mech. Engrg.*, 268:782–800, 2014.
- [34] A. Linke, G. Matthies, and L. Tobiska. Robust arbitrary order mixed finite element methods for the incompressible Stokes equations with pressure independent velocity errors. *ESAIM: Math. Model. Numer. Anal.*, 50(1):289–309, 2016.
- [35] A. Linke and C. Merdon. On velocity errors due to irrotational forces in the Navier–Stokes momentum balance. *J. Comput. Phys.*, 313:654–661, 2016.
- [36] A. Linke and C. Merdon. Pressure-robustness and discrete Helmholtz projectors in mixed finite element methods for the incompressible Navier–Stokes equations. *Comput. Methods Appl. Mech. Engrg.*, 311:304–326, 2016.
- [37] M. Olshanskii and L. G. Rebholz. Note on helicity balance of the Galerkin method for the 3D Navier–Stokes equations. *Comput. Methods Appl. Mech. and Engrg.*, 199(17):1032–1035, 2010.
- [38] M. A. Olshanskii. A low order Galerkin finite element method for the Navier–Stokes equations of steady incompressible flow: a stabilization issue and iterative methods. *Comput. Methods Appl. Mech. Engrg.*, 191(47):5515–5536, 2002.
- [39] M. A. Olshanskii and L. G. Rebholz. Longer time accuracy for incompressible Navier–Stokes simulations with the EMAC formulation. *Comput. Methods Appl. Mech. Engrg.*, 372:113369, 2020.
- [40] M. A. Olshanskii and A. Reusken. Grad-div stabilization for Stokes equations. *Math. Comp.*, 73:1699–1718, 2004.
- [41] A. Palha and M. Gerritsma. A mass, energy, enstrophy and vorticity conserving (MEEVC) mimetic spectral element discretization for the 2D incompressible Navier–Stokes equations. *J. Comput. Phys.*, 328:200–220, 2017.
- [42] L. G. Rebholz. An energy- and helicity-conserving finite element scheme for the Navier–Stokes equations. *SIAM J. Numer. Anal.*, 45(4):1622–1638, 2007.
- [43] O. Schenk, K. Gärtner, W. Fichtner, and A. Stricker. PARDISO: a high-performance serial and parallel sparse linear solver in semiconductor device simulation. *Future Gener. Comput. Syst.*, 18(1):69–78, 2001.
- [44] P. W. Schroeder, V. John, P. L. Lederer, C. Lehrenfeld, G. Lube, and J. Schöberl. On reference solutions and the sensitivity of the 2d Kelvin–Helmholtz instability problem. *Computers & Mathematics with Applications*, 77(4):1010–1028, feb 2019.
- [45] P. W. Schroeder, C. Lehrenfeld, A. Linke, and G. Lube. Towards computable flows and robust estimates for inf-sup stable FEM applied to the time-dependent incompressible Navier–Stokes equations. *SeMA J.*, 75(4):629–653, 2018.
- [46] J. Wang and X. Ye. New finite element methods in computational fluid dynamics by H(div) elements. *SIAM J. Numer. Anal.*, 45(3):1269–1286, 2007.
- [47] S. Zhang. A new family of stable mixed finite elements for the 3D Stokes equations. *Math. Comp.*, 74(250):543–554, 2005.
- [48] S. Zhang. Divergence-free finite elements on tetrahedral grids for $k \geq 6$. *Math. Comp.*, 80(274):669–695, 2011.
- [49] S. Zhang. Quadratic divergence-free finite elements on Powell–Sabin tetrahedral grids. *Calcolo*, 48(3):211–244, 2011.

GULF UNIVERSITY FOR SCIENCE AND TECHNOLOGY, BLOCK 5, BUILDING 1, MUARAK AL-ABDULLAH AREA, WEST MISHREF KUWAIT AND WEIERSTRASS INSTITUTE FOR APPLIED ANALYSIS AND STOCHASTICS (WIAS), MOHRENSTR. 39, 10117 BERLIN, GERMANY

Email address: ahmed.n@gust.edu.kw

WEIERSTRASS INSTITUTE FOR APPLIED ANALYSIS AND STOCHASTICS (WIAS), MOHRENSTR. 39, 10117 BERLIN, GERMANY AND FREIE UNIVERSITÄT BERLIN, DEPARTMENT OF MATHEMATICS AND COMPUTER SCIENCE, ARNIMALLEE 6, 14195 BERLIN, GERMANY

Email address: john@wias-berlin.de, ORCID 0000-0002-2711-4409

SCHOOL OF MATHEMATICS, SHANDONG UNIVERSITY, JINAN 250100, CHINA

Email address: xulisdu@126.com

WEIERSTRASS INSTITUTE FOR APPLIED ANALYSIS AND STOCHASTICS (WIAS), MOHRENSTR. 39, 10117 BERLIN, GERMANY

Email address: merdon@wias-berlin.de